NASA TECHNICAL NOTE
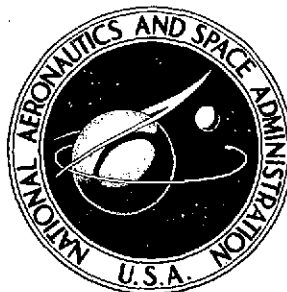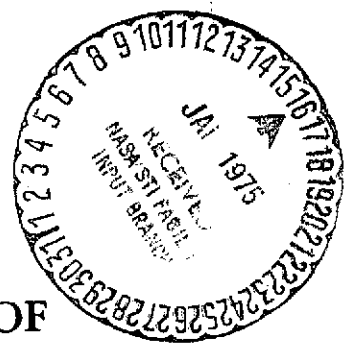
NASA TN D-7790

NASA TN D-7790

MOVING-BASE VISUAL SIMULATION STUDY OF DECOUPLED CONTROLS DURING APPROACH AND LANDING OF A STOL TRANSPORT AIRCRAFT

by G. Kimball Miller, Jr., and Perry L. Deal

Langley Research Center
Hampton, Va. 23665

NATIONAL AERONAUTICS AND SPACE ADMINISTRATION • WASHINGTON, D. C. • JANUARY 1975

1. Report No. NASA TN D-7790	2. Government Accession No.	3. Recipient's Catalog No.
4. Title and Subtitle MOVING-BASE VISUAL SIMULATION STUDY OF DECOUPLED CONTROLS DURING APPROACH AND LANDING OF A STOL TRANSPORT AIRCRAFT		5. Report Date January 1975
		6. Performing Organization Code
7. Author(s) G. Kimball Miller, Jr., and Perry L. Deal		8. Performing Organization Report No. L-9721
9. Performing Organization Name and Address NASA Langley Research Center Hampton, Va. 23665		10. Work Unit No. 505-06-93-02
		11. Contract or Grant No.
12. Sponsoring Agency Name and Address National Aeronautics and Space Administration Washington, D.C. 20546		13. Type of Report and Period Covered Technical Note
		14. Sponsoring Agency Code

15. Supplementary Notes

16. Abstract

A moving-base visual simulation study has been conducted to evaluate the use of decoupled controls during the approach and landing of an externally blown jet-flap STOL transport. The simulation employed all six rigid-body degrees of freedom and incorporated aerodynamic characteristics based on wind-tunnel data. The flight instrumentation included a localizer and a flight director. The primary piloting task was to capture and to maintain a two-segment glide slope by using the flight director. A closed-circuit television display of a STOLport provided visual cues during simulations of the approach and landing. The decoupled longitudinal controls used constant prefilter and feedback gains to provide steady-state decoupling of flight-path angle, pitch angle, and forward velocity. The pilots were enthusiastic about the decoupled longitudinal controls and believed that the simulator motion was an aid in evaluating the decoupled controls, although a minimum turbulence level with root-mean-square gust intensity of 0.3 m/sec (1 ft/sec) was required to mask undesirable characteristics of the moving-base simulator.

17. Key Words (Suggested by Author(s)) STOL handling qualities Decoupled control systems Terminal-area control	18. Distribution Statement Unclassified — Unlimited STAR Category 02	
19. Security Classif. (of this report) Unclassified	20. Security Classif. (of this page) Unclassified	21. No. of Pages 74	22. Price* $4.25

MOVING-BASE VISUAL SIMULATION STUDY OF DECOUPLED CONTROLS
DURING APPROACH AND LANDING OF A STOL TRANSPORT AIRCRAFT

By G. Kimball Miller, Jr., and Perry L. Deal
Langley Research Center

SUMMARY

A moving-base simulation study has been made to evaluate the use of decoupled controls during the approach and landing of an externally blown jet-flap STOL transport. The simulation employed all six rigid-body degrees of freedom and incorporated aerodynamic characteristics based on wind-tunnel data. The flight instrumentation included a localizer and a flight director. The primary piloting task was to capture and to maintain a two-segment glide slope by using the flight director. A closed-circuit television display of a STOLport provided visual cues during simulations of the approach and landing.

The decoupled longitudinal controls employed constant prefilter and feedback gains to provide steady-state decoupling of flight-path angle, pitch angle, and forward velocity as commanded through column, flap lever, and thrust lever, respectively. Two sets of control gains were examined. Although the first set of gains provided satisfactory handling qualities, the second set was chosen to significantly reduce the aircraft response to turbulence. The research pilot rated the piloting task equal for the two sets of gains and stated that the smoother ride produced by the second set of gains felt like that of a larger airplane. With either set of gains, the decoupled longitudinal controls were given a pilot rating of 3 or better for performing decelerating approaches from 120 knots to 70 knots. A pilot rating of 2 was given for the initial phase of a normal approach because of the ease with which the desired glide slope could be attained. The pilot rating for the critical flare-to-landing maneuver was also 2 or better because of the precision with which flight-path angle could be controlled in ground effect. In the lateral mode, decoupled control of yaw rate and sideslip angle was given a pilot rating of 2.

Although a minimum turbulence level with root-mean-square gust intensity of 0.3 m/sec (1 ft/sec) was required to mask erroneous acceleration spikes due to undesirable motion-base characteristics, the research pilot believed that the simulator motion was an aid in evaluating the decoupled control system.

INTRODUCTION

One method for obtaining the high lift coefficients required for the low approach and landing speeds of short take-off and landing (STOL) transport aircraft is the use of externally blown jet flaps. (See refs. 1, 2, and 3.) The operational requirements of STOL transport aircraft necessitate precise control capabilities. At the same time STOL aircraft handling qualities are poor compared with those of conventional aircraft, primarily because the period of the phugoid mode is much shorter than normal and the controls are more sluggish. Although conventional stability augmentation systems (SAS) have been applied to simulated externally blown flap STOL aircraft (refs. 4 and 5) to obtain satisfactory handling qualities, high pilot workloads still existed during the approach and landing. Consequently, a decoupled-control technique was investigated (ref. 6) with a fixed-base visual simulator.

In the longitudinal mode, the movement of the horizontal tail, flaps, symmetric spoilers, and throttle were automatically controlled to produce independent, or decoupled, control of flight-path angle, pitch angle, and forward velocity. In the lateral mode, the decoupled-control technique employed asymmetric spoilers, rudder, and ailerons to provide independent control of yaw rate and sideslip angle. The decoupled-control concept used constant prefilter and feedback gains which required no onboard computation. The use of constant gains was made possible by restricting the controller to the approach and landing phases and by requiring that the aircraft states be decoupled only under steady-state conditions. Modern control theory was then applied to determine the controls that would reach the steady state as efficiently as possible. In reference 6 the pilots concluded that the desired glide slope could be attained more easily with the decoupled longitudinal controls than with conventional controls and SAS and that the increased precision with which flight-path angle could be controlled in ground effect made the flare-to-landing maneuver more precise. In addition, the decoupled longitudinal controls permitted satisfactory performance of decelerating approaches from approximately 120 knots to 70 knots. However, in the fixed-base simulation certain decoupled longitudinal control gains and resulting aircraft accelerations in turbulence could vary considerably without affecting pilot opinion. Therefore the present investigation employed a moving-base simulator in an attempt to better define the decoupled longitudinal control gains under the influence of turbulence.

The current study employed the same simulation program, including decoupled lateral controls, as reference 6. The lateral control gains used in the fixed-base simulation were satisfactory and were not altered for this moving-base simulation. The simulation employed real-time digital computation of the six-degree-of-freedom nonlinear equations of motion representing the STOL aircraft aerodynamically described in references 1, 2, and 3. The study used a six-degree-of-freedom moving-base simulator

with the linear-filter washout logic described in reference 7 and included turbulence and ground effects. A visual display of a STOLport was generated by closed-circuit television.

SYMBOLS

Although values are given in both SI Units and U.S. Customary Units in this report, the measurements and calculations for the investigation were made in U.S. Customary Units.

A   matrix of aircraft stability derivatives

a_X, a_Y, a_Z body-axis longitudinal, lateral, and vertical accelerations, g units

B   matrix of aircraft-control coefficients

b   wing span

C   matrix relating desired output vector to state vector

C_l rolling-moment coefficient

C_m pitching-moment coefficient

C_n yawing-moment coefficient

C_T thrust coefficient

C_W aircraft weight in coefficient form, $\dfrac{-2mg}{\rho V^2 S}$

C_X longitudinal-force coefficient

C_Y side-force coefficient

C_Z normal-force coefficient

$\bar{c}$ mean aerodynamic chord, meters   (ft)

e_i	ith iteration of general variable e
F	matrix of feedback gains used in decoupled controller (see appendix A)
G	matrix of prefilter gains used in decoupled controller (see appendix A)
g	acceleration due to gravity, meters/second^2 (ft/sec^2)
h	altitude, meters (ft)
I	identity matrix
I_X, I_Y, I_Z	moments of inertia about X, Y, and Z body axes, kilogram-meters^2 (slug-ft^2)
I_{XZ}	product of inertia, kilogram-meters^2 (slug-ft^2)
J	performance index used in determining optimal control (see appendix A)
m	mass of airplane, kilograms (slugs)
n	number of flights
P	solution to matrix Riccati equation (see appendix A)
P_{ph}	period of phugoid mode, seconds
P_R	period of roll mode, seconds
P_{sp}	period of short-period longitudinal mode, seconds
p,q,r	angular velocities about X, Y, and Z body axes, degrees/second or radians/second
Q	state-variable weighting matrix used in performance index
R	control-variable weighting matrix used in performance index
R_a	range from aircraft to landing-approach beacon, measured on Earth's surface, meters (ft)

4

$\vec{r}$ vector of commanded inputs by pilot

S   wing area, meters^2 (ft^2)

s   Laplace operator

T   total thrust, newtons (lbf)

t   time, seconds

$(t_{1/2})_{ph}$ time to damp phugoid mode to one-half amplitude, seconds

$(t_{1/2})_R$ time to damp roll mode to one-half amplitude, seconds

$(t_{1/2})_{sp}$ time to damp short-period longitundinal mode to one-half amplitude, seconds

u,v,w   velocity components along X, Y, and Z body axes, meters/second or knots (ft/sec).

$\vec{u}$ vector of control variables

$\hat{u}$ difference between instantaneous control vector and vector of pilot inputs

V   airspeed, knots (ft/sec)

X,Y,Z   body axes

x,y,z   displacements of moving-base simulator in longitudinal, lateral, and vertical directions, meters (ft)

$\vec{x}$ instantaneous vector of state variables

$\vec{x_e}$ vector of state variables at equilibrium conditions

$\hat{x}$ difference between instantaneous and equilibrium state vectors

$\vec{y}$ vector of state variables to be controlled in a decoupled manner

z_{lg} — distance of landing gear from airplane center of gravity along Z body axis, meters (ft)

α — angle of attack, degrees

β — angle of sideslip, degrees

γ — flight-path angle, degrees

δ_a — aileron deflection, positive for right roll, degrees or radians

$\delta_{f1}, \delta_{f2}, \delta_{f3}$ — deflections of forward, middle, and rearward segments of trailing-edge flap, degrees or radians (see fig. 2)

$\delta_{\overline{f3}} = \delta_{f3} - 60^\circ$

δ_r — rudder deflection, degrees or radians

δ_s — asymmetric deflection of spoilers, positive for right roll, degrees or radians

δ_{sp} — symmetric spoiler deflection, degrees or radians

δ_t — horizontal-tail deflection, degrees or radians

δ_{th} — throttle deflection

ϵ_z — glide-slope error, $\tan^{-1}\left(\dfrac{h - z_{lg}}{R_a}\right) - \theta_{gs}$, degrees

ζ_{ph} — phugoid-mode damping ratio

ζ_R — roll-mode damping ratio

ζ_{sp} — short-period longitudinal-mode damping ratio

θ_{gs} — glide slope of landing-approach beacon, degrees

μ arithmetic mean, $\dfrac{\displaystyle\sum_{i=1}^{n} e_i}{n}$

ρ air density, kilograms/meter^3 (slugs/ft^3)

σ standard deviation, $\left[\dfrac{\displaystyle\sum_{i=1}^{n} (e_i - \mu)^2}{n - 1}\right]^{1/2}$

ψ, θ, φ Euler angles of rotation relating body and inertial axes, referred to as yaw, pitch, and roll, degrees or radians

ω_{ph} phugoid natural frequency, radians/second

ω_R rolling natural frequency, radians/second

ω_{sp} longitudinal short-period natural frequency, radians/second

Aircraft stability and control coefficients:

$$C_{l_\beta} = \frac{\partial C_l}{\partial \beta} \qquad\qquad C_{n_\beta} = \frac{\partial C_n}{\partial \beta} \qquad\qquad C_{Y_\beta} = \frac{\partial C_Y}{\partial \beta}$$

$$C_{X_{\delta_{f3}}} = \frac{\partial C_X}{\partial \delta_{f3}} \qquad\qquad C_{Z_{\delta_{f3}}} = \frac{\partial C_Z}{\partial \delta_{f3}} \qquad\qquad C_{m_{\delta_{f3}}} = \frac{\partial C_m}{\partial \delta_{f3}}$$

$$C_{X_{\delta_s}} = \frac{\partial C_X}{\partial \delta_s} \qquad\qquad C_{Z_{\delta_s}} = \frac{\partial C_Z}{\partial \delta_s} \qquad\qquad C_{m_{\delta_s}} = \frac{\partial C_m}{\partial \delta_s}$$

$$C_{l_{\delta_s}} = \frac{\partial C_l}{\partial \delta_s} \qquad\qquad C_{n_{\delta_s}} = \frac{\partial C_n}{\partial \delta_s} \qquad\qquad C_{Y_{\delta_s}} = \frac{\partial C_Y}{\partial \delta_s}$$

$$C_{X_{\delta_{sp}}} = \frac{\partial C_X}{\partial \delta_{sp}}$$

$$C_{Z_{\delta_{sp}}} = \frac{\partial C_Z}{\partial \delta_{sp}}$$

$$C_{m_{\delta_{sp}}} = \frac{\partial C_m}{\partial \delta_{sp}}$$

$$C_{X_{\delta_t}} = \frac{\partial C_X}{\partial \delta_t}$$

$$C_{Z_{\delta_t}} = \frac{\partial C_Z}{\partial \delta_t}$$

$$C_{m_{\delta_t}} = \frac{\partial C_m}{\partial \delta_t}$$

$$C_{l_{\delta_r}} = \frac{\partial C_l}{\partial \delta_r}$$

$$C_{n_{\delta_r}} = \frac{\partial C_n}{\partial \delta_r}$$

$$C_{Y_{\delta_r}} = \frac{\partial C_Y}{\partial \delta_r}$$

$$C_{l_{\delta_a}} = \frac{\partial C_l}{\partial \delta_a}$$

$$C_{n_{\delta_a}} = \frac{\partial C_n}{\partial \delta_a}$$

$$C_{Y_{\delta_a}} = \frac{\partial C_Y}{\partial \delta_a}$$

$$C_{l_p} = \frac{\partial C_l}{\partial \frac{pb}{2V}}$$

$$C_{n_p} = \frac{\partial C_n}{\partial \frac{pb}{2V}}$$

$$C_{Y_p} = \frac{\partial C_Y}{\partial \frac{pb}{2V}}$$

$$C_{l_r} = \frac{\partial C_l}{\partial \frac{rb}{2V}}$$

$$C_{n_r} = \frac{\partial C_n}{\partial \frac{rb}{2V}}$$

$$C_{Y_r} = \frac{\partial C_Y}{\partial \frac{rb}{2V}}$$

$$C_{X_u} = \frac{\partial C_X}{\partial \frac{u}{V}}$$

$$C_{Z_u} = \frac{\partial C_Z}{\partial \frac{u}{V}}$$

$$C_{m_u} = \frac{\partial C_m}{\partial \frac{u}{V}}$$

$$C_{X_\alpha} = \frac{\partial C_X}{\partial \alpha}$$

$$C_{Z_\alpha} = \frac{\partial C_Z}{\partial \alpha}$$

$$C_{m_\alpha} = \frac{\partial C_m}{\partial \alpha}$$

$$C_{X_q} = \frac{\partial C_X}{\partial \frac{q\bar{c}}{2V}}$$

$$C_{m_q} = \frac{\partial C_m}{\partial \frac{q\bar{c}}{2V}}$$

$$C_{Z_{\delta_{th}}} = \frac{\partial C_Z}{\partial \delta_{th}}$$

$$C_{X_{\dot{\alpha}}} = \frac{\partial C_X}{\partial \frac{\dot{\alpha}\bar{c}}{2V}}$$

$$C_{m_{\dot{\alpha}}} = \frac{\partial C_m}{\partial \frac{\dot{\alpha}\bar{c}}{2V}}$$

$$C_{Y_\varphi} = \frac{\partial C_Y}{\partial \varphi}$$

Superscripts:

T   matrix transpose

-1   matrix inverse

'   nondimensional perturbations from equilibrium

Subscripts:

c   commanded by pilot

g   gust intensity

$\dot{h}$ sink rate

x   touchdown position relative to runway threshold, positive down runway

0   trim condition

Abbreviations:

rms   *root mean square*

STOL   short take-off and landing

A dot over a symbol denotes differentiation with respect to time.

SIMULATED-AIRPLANE DESCRIPTION

The STOL airplane simulated in this study is the clustered-engine aircraft simulated in references 5 and 6 and aerodynamically described in references 1, 2, and 3. The airplane is a high-wing jet transport with four high-bypass-ratio turbofan engines. (See fig. 1.) The four engines yielded a maximum total thrust of 147 058 N (33 060 lbf). The engine response characteristics are given in table I.

For the approach and landing condition, the wing leading-edge flaps were deflected 60°, and the three segments of the full-span triple-slotted trailing-edge flaps were set at 25°, 10°, and 60°, respectively. (See fig. 2.) In the present investigation only deflec-

tion of the rear flap segment δ_{f3} was varied for control. The inboard elements of the flaps (fig. 1) were used as ailerons because they were more effective in providing rolling moments than the other flap elements (ref. 1). The physical characteristics of the simulated aircraft, including maximum control-surface deflection and deflection rate, are presented in table II. A time lag of 0.1 sec (ref. 5) was employed for all control surfaces to account for system delays. Table III contains the aerodynamic characteristics.

DECOUPLED CONTROL

Decoupled controls were employed throughout the current study in both the longitudinal and lateral modes. In the longitudinal mode the mechanization of the decoupled controls employed throttle, horizontal tail, flaps, and symmetric spoilers as active control elements. Four active control elements were used because doing so minimized the transients experienced during decelerating approaches with three active control elements. (See ref. 6.) As in reference 6, the rudder, ailerons, and asymmetric spoilers were used to provide decoupled control of yaw rate and sideslip angle.

The general approach for providing independent, or decoupled, longitudinal control of flight-path angle, pitch angle, and forward velocity is depicted in the following sketch:
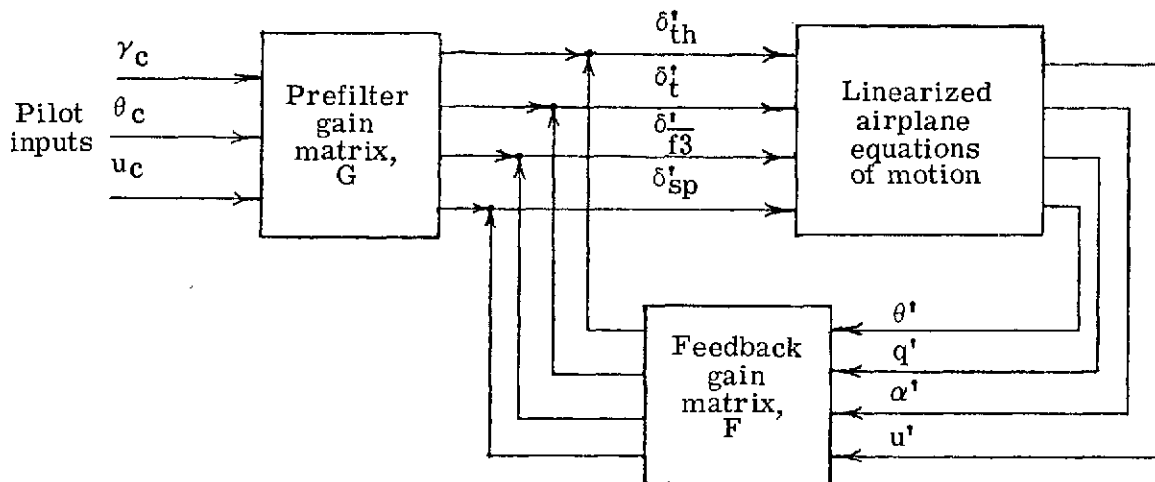
The decoupled controller was mechanized so that the pilot could command flight-path angle γ_c through inputs to the column, pitch angle θ_c through the flap lever, and forward velocity u_c through the thrust lever. Although this mechanization was used in both the fixed-base and moving-base simulation studies, a possible problem during emergency wave-off was noted in the fixed-base study (ref. 6). The potential problem concerned the tendency of a pilot trained on conventional controls to push the thrust lever full forward for an emergency wave-off combined with the tendency of the decoupled longitudinal controls to cause transients in sink rate when a large increase in velocity is commanded. Thus, it may be desirable to use some lever other than the thrust lever for

commanding forward velocity. The thumb-wheel controller on the left horn of the control yoke was used to trim flight-path angle so that the pilot would not be required to hold the column forward for a descent maneuver. With decoupled controls the aircraft pitch angle, pitch rate, angle of attack, and forward velocity must be continuously measured. In this simulation study the measurements were assumed to be perfect.

The feedback gain matrix F and prefilter gain matrix G result in the aircraft control elements moving to produce decoupled control as commanded by the pilot. There are a number of ways to obtain the feedback and prefilter gain matrices required for decoupled control. The most versatile method would be the use of an onboard computer to find the time-varying adaptive gains. A simplified approach was taken in the present investigation. Requiring that the commanded aircraft states be decoupled only in the steady-state case and restricting the controller to the approach and landing phase of operations permitted the use of constant prefilter and feedback gains and avoided onboard computation. (See appendix A.) The control gains of either the lateral or the longitudinal decoupled system could be changed after each flight by changing the weighting matrices in the performance index (appendix A) as a function of pilot opinion. Decoupled longitudinal controls and decoupled lateral controls are developed in appendix A and in appendix B, respectively.

SIMULATION EQUIPMENT

The digital-computer program used in the present simulation employed nonlinear equations of motion for six rigid-body degrees of freedom. The turbulence model used in the study was based on the Dryden spectral form (ref. 5) having rms gust-intensity values up to 1.2 m/sec (4 ft/sec).

The single-degree-of-freedom performance limits of the six-degree-of-freedom moving-base simulator (fig. 3) used in the current study are presented in table IV. The constraint or washout logic presented in reference 7 was considered to be state of the art and was used to constrain the simulated aircraft excursions to the limit of the simulator. The values used for the washout parameters of the constraint logic were determined subjectively by the research pilot and are presented in table V. The definition of each washout parameter has meaning only in the context of reference 7 and may be found therein.

The transport-type cockpit (fig. 4) was equipped with conventional flight and engine-thrust control devices. The simulator control forces were provided by a hydraulic servosystem as functions of control displacement and rate. The characteristics of the simulator control system were different from those used in references 5 and 6 and are presented in table VI. The flight instrument display was representative of current trans-

port aircraft. Instruments indicating angle of attack, sideslip angle, and flap angle were included. The localizer channel of the conventional cross-pointer-type flight director was driven in the manner described in appendix A of reference 5. The glide-slope channel was driven by the raw glide-slope error ϵ_z.

The visual cues for flare and landing were obtained by means of a 675-scan-line color television camera and with an optical pickup similar to that described in reference 8. The optical pickup was driven by the output of the moment equations to provide the three rotational degrees of freedom of the aircraft. The three translational degrees of freedom were obtained by mounting the optical pickup and television camera on a transport system that moved relative to a terrain model in response to the output of the force equations. The terrain model (fig. 5) was a three-dimensional 1/300-scale model of the area around a STOLport. The visual display was presented to the pilot through a television monitor and collimating lens system mounted in the pilot's windshield. Each flight was terminated at touchdown.

TEST PROGRAM

The flight instrumentation included a localizer and a flight director. The pilot's task was to assume command of the aircraft in level flight and to perform a two-segment approach using the flight director. The flights were initiated at an altitude of approximately 243.8 m (800 ft), at varying distances from the runway (with the airplane initially below the glide slope), and with lateral offsets up to 61 m (200 ft) from the runway center line. The pilot was instructed to visually acquire the 914-m (3000-ft) runway and to land in a designated area with sink rates of less than 1 m/sec (3 ft/sec). The touchdown zone marked on the runway (fig. 6) was 137.2 m (450 ft) long. The basic restrictions on the flights were that the angle of attack for approach conditions must be at least 10° below the stall and the approach speed must be at least 15 knots greater than the critical engine-out stall speed. The normal approach, performed at 70 knots, was a two-segment approach in which a 6° glide slope was followed to an altitude of 61 m (200 ft). At this altitude a transition was made to a 4° glide slope. In a number of flights the pilots were required to decelerate from approximately 120 knots to 70 knots while maintaining the desired glide slope. The adverse ground effects employed in reference 5 were used. These ground effects caused a nose-down pitching moment and a decrease in lift and drag as the ground was approached. Although a research pilot and a research engineer were pilots during the study, only the research pilot rated the control systems.

RESULTS AND DISCUSSION

The hydraulic servosystem providing control forces in the current moving-base simulation had operating characteristics that were different from those of the servosystem employed in the fixed-base simulation (ref. 6). Consequently, a preliminary series of flights was performed with the moving-base simulator in a fixed-base mode in order to assess the effects of the differences in control-force systems on the pilot's ability to achieve the desired touchdown conditions. The prefilter and feedback gain matrices used are those which the pilots believed provided the best response during the fixed-base simulation study. These gains and the resulting stability characteristics are presented in table VII. The touchdown conditions obtained with the moving-base simulator in a fixed-base mode are presented in table VIII for comparison with the touchdown conditions obtained during the fixed-base study of reference 6. Table VIII reflects the difference between the two control-force servosystems. The results in this table should, however, be conservative since difficulty in judging altitude and altitude rate historically exists in simulations using closed-circuit television for image generation. Because of this difficulty, sink rates at touchdown for visual simulations are generally higher than those experienced in flight. The research pilot stated that simulation landings, compared with actual landings, were adversely affected by the lack of important visual cues, such as peripheral vision, depth perception, and resolution.

Operational Characteristics of Moving-Base Simulator

Operating characteristics of the moving-base simulator can best be examined by consideration of the aircraft response characteristics for the decoupled longitudinal controls. However, the response characteristics of the decoupled controls are different from those associated with conventional controls because the pitch angle θ_c is independent of the primary control γ_c. The time history presented in figure 7 shows aircraft response for typical control inputs. In this flight the pilot set up a glide slope of almost 6^0, commanded a pitch angle change after 18 sec, reversed the command at 31 sec, and then removed the command at 43 sec. Approximately 52 sec into the flight, the forward velocity was reduced by about 8.9 knots in 3 sec by means of the velocity controller. Although aircraft response to pitch commands was fairly sluggish, the primary longitudinal control with decoupled controls is regulation of flight-path angle. A commanded change in flight-path angle 68 sec into the flight resulted in a change in γ of at least 5^0 in 1 sec. The aircraft accelerations due to all control inputs were relatively moderate, the largest being a vertical acceleration of about 1/4g when the flight-path angle was pulsed at 68 sec.

The acceleration profiles in figure 7 are those computed for the aircraft. The acceleration profiles actually experienced by the simulator pilot (fig. 8) were obtained

from an accelerometer package installed in the cockpit. The actual accelerations which the simulator pilot felt were somewhat noisy and contained erroneous spikes that were large compared with commanded accelerations. Although the source of these erroneous acceleration spikes was never adequately determined, they appeared to occur whenever the legs of the moving-base simulator reversed their direction of motion. (See ref. 10.) Interaction of the six legs of the moving-base simulator caused the erroneous accelerations to crossfeed into all degrees of freedom of the simulator. For example, the lateral mode had no inputs during the flight shown in figure 7, whereas the lateral accelerations measured for the moving-base simulator (fig. 8) were as large as 0.07g. The erroneous accelerations were quite objectionable to the simulator pilots during flights in still air. However, the pilots' objections could be removed by using low-level turbulence to mask the erroneous accelerations of the simulator. Consequently, all flights performed on the moving-base simulator included turbulence with an rms gust intensity of at least 0.3 m/sec (1 ft/sec).

The computed aircraft accelerations and the accelerations from the washout computations which drive the moving-base simulator are presented in figure 9 for a typical series of control inputs. The accelerations after the washout computations do not have the acceleration spikes.

Landings Using Motion Cues

The time history of a typical decelerating approach in turbulence with an rms gust intensity of 0.3 m/sec (1 ft/sec) is presented in figure 10 for a two-segment approach in which the desired glide slope changes from 6° to 4° at an altitude of approximately 61 m (200 ft). The flight was initiated with the airplane in level flight at a speed of 120 knots and below the 6° glide-slope signal. Approximately 4 sec into the flight the pilot began simultaneously to acquire the desired 6° glide slope and to reduce the forward velocity to about 70 knots. The pilot made the transition to the 4° glide slope after about 47 sec of flight and then landed in the designated 137.2-m-long (450-ft) landing area with a sink rate of about 1.8 m/sec (6 ft/sec). The computed performance of the moving-base simulator during this flight is presented in figure 11. The washout parameters were sized to maximize the longitudinal acceleration response during decelerating approaches at the expense of the vertical accelerations. Thus, the vertical channel was scaled by 0.2 because the x-y envelope was inversely proportional to vertical displacement. A second compromise involved the coordination of longitudinal channel and pitch channel. The washout parameters could be chosen so that the longitudinal accelerations experienced on the moving-base simulator during the deceleration maneuver would be similar to the flight accelerations. To do so, however, would result in pitch rates that would be objectionable to the pilot. The compromise

14

washout parameters yielded longitudinal accelerations, typified by those of figure 11, which the pilots believe are quite realistic. In addition, the amount of erroneous pitch rate exhibited in figure 11 was not objectionable to the pilots.

Although the limited displacement of the moving-base simulator prohibited duplication of the flight acceleration profiles, the research pilot believed that this motion was an aid in evaluating the decoupled control system. The pilot ratings (of the form presented in table IX), however, were not changed by inclusion of motion cues. The decoupled longitudinal controls were given a pilot rating of 3 or better for performing decelerating approaches. The pilot gave the decoupled longitudinal controls a rating of 2 for the initial approach because of the ease with which the desired glide slope could be attained. The pilot rating for the flare-to-landing maneuver was 2 or better because of the precision with which flight-path angle could be controlled in ground effect. The decoupled lateral controls were given a pilot rating of 2 as in the fixed-base study (ref. 6). The touchdown conditions obtained with the decoupled longitudinal and lateral control systems are presented in table X in which the results of the research pilot and the research engineer are combined because no significant difference existed between these men as pilots. The addition of motion cues had little effect on the touchdown conditions. (See table VIII(b).) The pilots believed that the difficulty in landing in the designated area with low sink rates was primarily a result of visual display limitations.

Influence of Turbulence on Decoupled Control System

Aircraft vertical and longitudinal acceleration levels for a typical constant-speed two-segment approach in turbulence with an rms gust intensity of 0.3 m/sec (1 ft/sec) are presented in figure 12. The acceleration profiles generated by the washout logic are presented in figure 13. Although the acceleration levels experienced with the decoupled controls were not objectionable, the vertical and longitudinal components were believed to be unnecessarily high. Therefore, the weights of the performance index were altered on the basis of pilot opinion until the decoupled longitudinal control system gave a ride that was noticeably smoother but still handled satisfactorily. The resulting prefilter and feedback gain matrices are presented in table XI with the corresponding airplane stability characteristics. The time history of a typical constant-speed two-segment approach in turbulence with an rms gust intensity of 0.3 m/sec (1 ft/sec) with the modified decoupled controls is presented in figure 14. Although the aircraft response to turbulence was significantly reduced by the new feedback and prefilter gains (compare figs. 12 and 14), the pilot merely felt as if he were flying a larger airplane with good handling qualities. The pilot ratings consequently were unchanged. It should be noted that, in addition to the normal constant-speed approaches, the pilot ratings are based on decelerating approaches, approaches with initial lateral offsets, and approaches in crosswinds. The normal constant-speed approaches presented in figures 12 and 14 were

chosen because they best exemplify the differences in longitudinal and vertical accelerations achieved with the two sets of gains. As previously stated, the lateral decoupled control gains were not varied during the study. The apparent differences in the lateral controls shown in figures 12 and 14 are the result of piloting differences. The acceleration profiles generated by the washout logic are presented in figure 15 for comparison with those of the original decoupled longitudinal control gains shown in figure 13.

The touchdown conditions obtained with the smoother riding decoupled control gains are presented in table XII and are comparable with those obtained with the original gains (table X), even though the smoother riding airplane was less responsive to control inputs.

CONCLUDING REMARKS

A moving-base simulation study has been conducted to evaluate the use of decoupled controls during the approach and landing of an externally blown jet-flap STOL transport. The decoupled longitudinal controls employed the throttle, horizontal tail, flaps, and symmetric spoilers as active control elements to provide steady-state decoupling of flight-path angle, pitch angle, and forward velocity as commanded through column, flap lever, and thrust lever, respectively. Restricting the application of decoupled control to the steady-state case and to the approach and landing phase of operations permitted the use of constant prefilter and feedback gains and avoided onboard computation. The flight instrumentation included a localizer and a flight director. The piloting task was to capture and to maintain a two-segment glide slope by using the flight director until visually landing in an area 137.2 m (450 ft) long on the end of a runway.

Two different sets of prefilter and feedback gains for longitudinal decoupling were examined. The first set of gains were those employed in the original fixed-base simulation study to obtain satisfactory handling qualities, and the second set of gains were chosen to significantly reduce the aircraft response to turbulence. Although the airplane response to turbulence was reduced with the second set of gains, the pilot ratings of the aircraft handing qualities were unchanged. The research pilot stated that the smoother riding airplane merely seemed like a larger airplane with satisfactory handling qualities. With either set of gains the decoupled longitudinal controls were given a pilot rating of 3 or better for performing decelerating approaches. In addition, these controls were given a pilot rating of 2 for the initial phase of normal approaches because of the ease with which the desired glide slope could be attained. The pilot rating for the flare-to-landing maneuver was 2 or better because of the precision with which flight-path angle could be controlled in ground effect. In the lateral mode, decoupled control of yaw rate and sideslip angle was given a pilot rating of 2.

16

Although a minimum turbulence level with root-mean-square gust intensity of 0.3 m/sec (1 ft/sec) was required to mask erroneous acceleration spikes due to undesirable characteristics of the moving-base simulator, the pilot believed that the simulator motion is an aid in evaluating the decoupled control system.

Langley Research Center,
National Aeronautics and Space Administration,
Hampton, Va., November 19, 1974.

APPENDIX A

DECOUPLED LONGITUDINAL CONTROLS

The three longitudinal equations of motion were linearized as perturbations about an equilibrium condition in equations (1-59) of reference 11. These three equations can be nondimensionalized with respect to time using

$$t' = \frac{u_0}{\bar{c}} t \tag{A1}$$

and solved simultaneously to give

$$\frac{d^2\theta'}{dt'^2} = \frac{1}{2\mu K_Y^2}\left[\left(\frac{C_{m_q} + C_{m_{\dot{\alpha}}}}{2}\right)\frac{d\theta'}{dt'} + \left(C_{m_\alpha} + \frac{C_{m_{\dot{\alpha}}}C_{Z_\alpha}}{4\mu}\right)\alpha' + \left(C_{m_u} + \frac{C_{m_{\dot{\alpha}}}C_{Z_u}}{4\mu}\right)u'\right.$$

$$\left. + \left(C_{m_{\delta_t}} + \frac{C_{m_{\dot{\alpha}}}C_{Z_{\delta_t}}}{4\mu}\right)\delta_t' + \left(C_{m_{\delta_{\overline{f3}}}} + \frac{C_{m_{\dot{\alpha}}}C_{Z_{\delta_{\overline{f3}}}}}{4\mu}\right)\delta_{\overline{f3}}' + \left(C_{m_{\delta_{sp}}} + \frac{C_{m_{\dot{\alpha}}}C_{Z_{\delta_{sp}}}}{4\mu}\right)\delta_{sp}'\right] \tag{A2}$$

$$\frac{d\alpha'}{dt'} = \frac{1}{2\mu}\left(2\mu\frac{d\theta'}{dt'} + C_{Z_\alpha}\alpha' + C_{Z_u}u' + C_{Z_{\delta_t}}\delta_t' + C_{Z_{\delta_{\overline{f3}}}}\delta_{\overline{f3}}' + C_{Z_{\delta_{sp}}}\delta_{sp}'\right) \tag{A3}$$

$$\frac{du'}{dt'} = \frac{1}{2\mu}\left[C_W\theta' + \left(\frac{C_{X_q} + C_{X_{\dot{\alpha}}}}{2}\right)\frac{d\theta'}{dt'} + \left(C_{X_\alpha} + \frac{C_{X_{\dot{\alpha}}}C_{Z_\alpha}}{4\mu}\right)\alpha' + \left(C_{X_u} + \frac{C_{X_{\dot{\alpha}}}C_{Z_u}}{4\mu}\right)u'\right.$$

$$+ \left(C_T + \frac{C_{X_{\dot{\alpha}}}C_{Z_{\delta_{th}}}}{4\mu}\right)\delta_{th}' + \left(C_{X_{\delta_t}} + \frac{C_{X_{\dot{\alpha}}}C_{Z_{\delta_t}}}{4\mu}\right)\delta_t' + \left(C_{X_{\delta_{\overline{f3}}}} + \frac{C_{X_{\dot{\alpha}}}C_{Z_{\delta_{\overline{f3}}}}}{4\mu}\right)\delta_{\overline{f3}}'$$

$$\left. + \left(C_{X_{\delta_{sp}}} + \frac{C_{X_{\dot{\alpha}}}C_{Z_{\delta_{sp}}}}{4\mu}\right)\delta_{sp}'\right] \tag{A4}$$

where the primed parameters are perturbations from the equilibrium or trim conditions of the airplane in nondimensional form; that is

$$\theta' = \theta - \theta_0 \tag{A5}$$

$$\alpha' = \alpha - \alpha_0 = \frac{w - w_0}{u_0} \tag{A6}$$

$$u' = \frac{u - u_0}{u_0} \tag{A7}$$

and where

$$\mu = \frac{m}{\rho S \bar{c}} \tag{A8}$$

$$K_Y{}^2 = \frac{I_Y}{m \bar{c}^2} \tag{A9}$$

The mass and dimensional characteristics of the simulated airplane are presented in table II and the basic aerodynamic coefficients in table III. Constant coefficients were employed in the linearized longitudinal equations of motion corresponding to an angle of attack of 10°, a forward velocity of 70 knots, and a thrust coefficient of 1.87.

The linearized longitudinal equations of motion can be written in state vector notation as

$$\dot{\vec{x}} = A\vec{x} + B\vec{u} \tag{A10}$$

where the state vector is

$$\vec{x} = \begin{bmatrix} \theta' \\ \dot{\theta}' \\ \alpha' \\ u' \end{bmatrix} \tag{A11}$$

and the control vector is

$$\vec{u} = \begin{bmatrix} \delta'_{th} \\ \delta'_t \\ \delta'_{f3} \\ \delta'_{sp} \end{bmatrix} \tag{A12}$$

The general control law is given as

$$\vec{u} = -F\vec{x} + G\vec{r} \tag{A13}$$

where $\vec{r}$ is the vector of commanded pilot inputs γ_c, θ_c, and u_c that are to be controlled in a decoupled manner. The output equation is

$$\vec{y} = C\vec{x} \tag{A14}$$

When equation (A13) is substituted into equation (A10), the Laplace transform of the result can be written as

$$\vec{x}(s) = (sI - A + BF)^{-1}BG\vec{r}(s) \tag{A15}$$

Substituting the Laplace transform of equation (A14) into equation (A15) and requiring that the output $\vec{y}(s)$ be equal to the commanded pilot input $\vec{r}(s)$ under steady-state conditions results in the prefilter gain

$$G = -\left[C(A - BF)^{-1}B\right]^{-1} \tag{A16}$$

Normally the bracketed term is nonsingular. There are cases, however, when all four control elements are used to decouple flight-path angle, pitch angle, and forward velocity, so that the bracketed term is singular. In this case the difference between the actual output $\vec{y}(s)$ and the commanded pilot input $\vec{r}(s)$ is minimized (approximately decoupled steady-state control) by using the pseudo inverse of $C(A - BF)^{-1}B$. Because this term has zeros in the fourth row, it can be written

$$C(A - BF)^{-1}B = TN \tag{A17}$$

where

$$T = \begin{bmatrix} 100 \\ 010 \\ 001 \\ 000 \end{bmatrix} \tag{A18}$$

and N is $C(A - BF)^{-1}B$ with the fourth row deleted. The pseudo inverse can then be written (ref. 12) as

$$G = -N^T\left(NN^T\right)^{-1}T^T \tag{A19}$$

Having obtained the prefilter gain matrix G required for approximately decoupled steady-state control, it is desirable to obtain the control that will reach that condition as efficiently as possible. Consequently, optimal control theory was employed to obtain the feedback gain matrix F.

For a given constant-pilot input $\vec{r}$, there is an associated equilibrium state $\overrightarrow{x_e}$ that is reached in the steady-state case; that is

$$0 = (A - BF)\overrightarrow{x_e} + BG\vec{r} \tag{A20}$$

which, since it is zero, can be subtracted from the closed-loop equations of motion,

$$\dot{\vec{x}} = (A - BF)\vec{x} + BG\vec{r} - \left[(A - BF)\vec{x_e} + BG\vec{r}\right] \qquad (A21)$$

where $\hat{x}$ is the difference between the instantaneous state $\vec{x}$ and the new equilibrium state $\vec{x_e}$. Equation (A21) is therefore

$$\dot{\hat{x}} = (A - BF)\hat{x} \qquad (A22)$$

which can be written as

$$\dot{\hat{x}} = A\hat{x} + B\hat{u} \qquad (A23)$$

where

$$\hat{u} = -F\hat{x} \qquad (A24)$$

which is the difference between the instantaneous control vector $\vec{u}$ and the pilot-control input associated with the new equilibrium state. The performance index

$$J = \int_0^\infty \left(\hat{x}^T Q \hat{x} + \hat{u}^T R \hat{u}\right) dt \qquad (A25)$$

and equation (A23) constitute the familiar state-regulator problem with quadratic performance index for which the optimal control $\hat{u}^*$ (ref. 13) is

$$\hat{u}^* = -R^{-1}B^T P\hat{x} \qquad (A26)$$

where P is the solution to the time invariant matrix Riccati equation

$$PA + A^T P - PBR^{-1}B^T P + Q = 0 \qquad (A27)$$

The particular solution for the Riccati equation is based on the iterative approach taken in reference 14.

Equating the general control $\hat{u}$ to the optimal control $\hat{u}^*$ permits the solution for the remaining unknown gain matrix

$$F = R^{-1}B^T P \qquad (A28)$$

The feedback gain F is optimal for a given set of weighting matrices Q and R in the performance index (eq. (A25)). The off-diagonal terms in these weighting matrices were zero, whereas the diagonal terms were varied as a function of pilot opinion as the simulation study progressed.

DECOUPLED LATERAL CONTROLS

The lateral equations of motion were linearized as perturbations about an equilibrium condition (ref. 11) as

$$\frac{d^2\varphi'}{dt'^2} = \frac{\bar{c}mb}{2\mu I_{XZ}} \left\{ \frac{b}{2\bar{c}} \left[\left(\frac{I_Z I_{XZ}}{I_Z^2 - I_{XZ}^2} \right) C_{l_p} + \left(\frac{I_Z I_X}{I_Z^2 - I_{XZ}^2} - 1 \right) C_{n_p} \right] \frac{d\varphi'}{dt'} + \frac{b}{2\bar{c}} \left[\left(\frac{I_Z I_{XZ}}{I_Z^2 - I_{XZ}^2} \right) C_{l_r} \right. \right.$$

$$+ \left. \left(\frac{I_Z I_X}{I_Z^2 - I_{XZ}^2} - 1 \right) C_{n_r} \right] \frac{d\psi'}{dt'} + \left[\left(\frac{I_Z I_{XZ}}{I_Z^2 - I_{XZ}^2} \right) C_{l_\beta} + \left(\frac{I_Z I_X}{I_Z^2 - I_{XZ}^2} - 1 \right) C_{n_\beta} \right] \beta'$$

$$+ \left[\left(\frac{I_Z I_{XZ}}{I_Z^2 - I_{XZ}^2} \right) C_{l_{\delta_r}} + \left(\frac{I_Z I_X}{I_Z^2 - I_{XZ}^2} - 1 \right) C_{n_{\delta_r}} \right] \delta_r' + \left[\left(\frac{I_Z I_{XZ}}{I_Z^2 - I_{XZ}^2} \right) C_{l_{\delta_a}} \right.$$

$$+ \left. \left(\frac{I_Z I_X}{I_Z^2 - I_{XZ}^2} - 1 \right) C_{n_{\delta_a}} \right] \delta_a' + \left[\left(\frac{I_Z I_{XZ}}{I_Z^2 - I_{XZ}^2} \right) C_{l_{\delta_s}} + \left(\frac{I_Z I_X}{I_Z^2 - I_{XZ}^2} - 1 \right) C_{n_{\delta_s}} \right] \delta_s' \right\} \tag{B1}$$

$$\frac{d^2\psi'}{dt'^2} = \frac{\bar{c}mb}{2\mu(I_Z^2 - I_{XZ}^2)} \left[\frac{b}{2\bar{c}} \left(I_{XZ} C_{l_p} + I_X C_{n_p} \right) \frac{d\varphi'}{dt'} + \frac{b}{2\bar{c}} \left(I_{XZ} C_{l_r} + I_X C_{n_r} \right) \frac{d\psi'}{dt'} \right.$$

$$+ \left(I_{XZ} C_{l_\beta} + I_X C_{n_\beta} \right) \beta' + \left(I_{XZ} C_{l_{\delta_r}} + I_X C_{n_{\delta_r}} \right) \delta_r' + \left(I_{XZ} C_{l_{\delta_a}} + I_X C_{n_{\delta_a}} \right) \delta_a'$$

$$+ \left. \left(I_{XZ} C_{l_{\delta_s}} + I_X C_{n_{\delta_s}} \right) \delta_s' \right] \tag{B2}$$

$$\frac{d\beta'}{dt'} = \frac{1}{2\mu} \left[C_{Y_\varphi} \varphi' + \frac{b}{2\bar{c}} C_{Y_p} \frac{d\varphi'}{dt'} + \left(\frac{b}{2\bar{c}} C_{Y_r} - 2\mu \right) \frac{d\psi'}{dt'} + C_{Y_\beta} \beta' + C_{Y_{\delta_r}} \delta_r' \right.$$

$$+ \left. C_{Y_{\delta_a}} \delta_a' + C_{Y_{\delta_s}} \delta_s' \right] \tag{B3}$$

where the primed parameters are perturbations from equilibrium conditions with

$$t' = \frac{u_0}{\bar{c}} t \tag{B4}$$

$$\mu = \frac{m}{\rho S \bar{c}} \tag{B5}$$

These linearized lateral equations of motion are then written in state vector notation as

$$\dot{\vec{x}} = A\vec{x} + B\vec{u} \tag{B6}$$

and the prefilter and feedback gain matrices required to decouple yaw rate and sideslip angle are determined as in appendix A.

REFERENCES

1. Parlett, Lysle P.; Greer, H. Douglas; Henderson, Robert L.; and Carter, C. Robert: Wind-Tunnel Investigation of an External-Flow Jet-Flap Transport Configuration Having Full-Span Triple-Slotted Flaps. NASA TN D-6391, 1971.

2. Grafton, Sue B.; Parlett, Lysle P.; and Smith, Charles C., Jr.: Dynamic Stability Derivatives of a Jet Transport Configuration With High Thrust-Weight Ratio and an Externally Blown Jet Flap. NASA TN D-6440, 1971.

3. Vogler, Raymond D.: Wind-Tunnel Investigation of a Four-Engine Externally Blowing Jet-Flap STOL Airplane Model. NASA TN D-7034, 1970.

4. Grantham, William D.; Sommer, Robert W.; and Deal, Perry L.: Simulator Study of Flight Characteristics of a Jet-Flap STOL Transport Airplane During Approach and Landing. NASA TN D-6225, 1971.

5. Grantham, William D.; Nguyen, Luat T.; Patton, James M., Jr.; Deal, Perry L.; Champine, Robert A.; and Carter, C. Robert: Fixed-Base Simulator Study of an Externally Blown Flap STOL Transport Airplane During Approach and Landing. NASA TN D-6898, 1972.

6. Miller, G. Kimball, Jr.; Deal, Perry L.; and Champine, Robert A.: Fixed-Base Simulation Study of Decoupled Controls During Approach and Landing of a STOL Transport Airplane. NASA TN D-7363, 1974.

7. Parrish, Russell V.; Dieudonne, James E.; and Martin, Dennis J., Jr.: Motion Software for a Synergistic Six-Degree-of-Freedom Motion Base. NASA TN D-7350, 1973.

8. Kaestner, P. T.: An Articulated Optical Pickup for Scale Model Simulation. J. SMPTE, vol. 76, no. 10, Oct. 1967, pp. 988-991.

9. Chase, Wendell D.: Evaluation of Several TV Display Systems for Visual Simulation of the Landing Approach. NASA TN D-6274, 1971.

10. Warton, L. H.: A Four Degrees of Freedom, Cockpit Motion Machine for Flight Simulation. R. & M. No. 3727, Brit. A.R.C., 1973.

11. Blakelock, John H.: Automatic Control of Aircraft and Missiles. John Wiley & Sons, Inc., c.1965.

12. Zadeh, Lotfi A.; and Desoer, Charles A.: Linear System Theory. McGraw-Hill Book Co., Inc., c.1963.

13. Athans, Michael; and Falb, Peter L.: Optimal Control. McGraw-Hill Book Co., Inc., c.1966.

14. Kleinman, David L.: On an Iterative Technique for Riccati Equation Computations. IEEE Trans. Automat. Contr., vol. AC-13, no. 1, Feb. 1968, pp. 114-115.

TABLE I.- SIMULATED ENGINE RESPONSE CHARACTERISTICS

(a) Acceleration

Time, sec	Thrust response, N (lbf), for T_C, N (lbf), of —										
	2611 (587)	6530 (1468)	13 625 (3063)	16 796 (3776)	22 023 (4951)	36 764 (8265)	6904 (1552)	14 741 (3314)	18 847 (4237)	21 649 (4867)	36 764 (8265)
0	1681 (378)	1681 (378)	1 681 (378)	1 681 (378)	1 681 (378)	1 681 (378)	2611 (587)	2 611 (587)	2 611 (587)	2 611 (587)	2 611 (587)
.2	1681 (378)	1681 (378)	1 681 (378)	1 681 (378)	1 681 (378)	1 681 (378)	2705 (608)	2 705 (608)	2 705 (608)	2 705 (608)	2 705 (608)
.4	1775 (399)	1775 (399)	1 775 (399)	1 775 (399)	1 775 (399)	1 775 (399)	2798 (629)	2 798 (629)	2 798 (629)	2 798 (629)	2 798 (629)
.6	1868 (420)	1868 (420)	1 868 (420)	1 868 (420)	1 868 (420)	1 868 (420)	2985 (671)	2 985 (671)	2 985 (671)	2 985 (671)	2 985 (671)
.8	2055 (462)	2055 (462)	2 055 (462)	2 055 (462)	2 055 (462)	2 055 (462)	3358 (755)	3 358 (755)	3 358 (755)	3 358 (755)	3 358 (755)
1.0	2144 (482)	2144 (482)	2 144 (482)	2 144 (482)	2 144 (482)	2 144 (482)	4106 (923)	4 106 (923)	4 106 (923)	4 106 (923)	4 106 (923)
1.2	2331 (524)	2331 (524)	2 331 (524)	2 331 (524)	2 331 (524)	2 331 (524)	5227 (1175)	5 227 (1175)	5 227 (1175)	5 227 (1175)	5 227 (1175)
1.4	2424 (545)	2611 (587)	2 611 (587)	2 611 (587)	2 611 (587)	2 611 (587)	5600 (1259)	7 090 (1594)	7 277 (1636)	7 277 (1636)	7 277 (1636)
1.6	2518 (566)	2985 (671)	2 985 (671)	2 985 (671)	2 985 (671)	2 985 (671)	5880 (1322)	10 449 (2349)	10 449 (2349)	10 449 (2349)	10 449 (2349)
1.8	2611 (587)	3545 (797)	3 545 (797)	3 545 (797)	3 545 (797)	3 545 (797)	6161 (1385)	11 196 (2517)	12 691 (2853)	12 691 (2853)	15 302 (3440)
2.0		4012 (902)	4 386 (986)	4 386 (986)	4 386 (986)	4 386 (986)	6343 (1426)	11 943 (2685)	14 372 (3231)	15 115 (3398)	18 473 (4153)
2.2		4666 (1049)	5 600 (1259)	5 600 (1259)	5 600 (1259)	5 600 (1259)	6437 (1447)	12 504 (2811)	15 489 (3482)	16 796 (3776)	21 649 (4867)
2.4		5040 (1133)	8 211 (1846)	8 211 (1846)	8 211 (1846)	8 211 (1846)	6623 (1489)	12 878 (2895)	16 329 (3671)	17 917 (4028)	24 447 (5496)
2.6		5600 (1259)	9 519 (2140)	11 383 (2559)	11 383 (2559)	11 383 (2559)	6717 (1510)	13 158 (2958)	16 983 (3818)	18 571 (4175)	26 876 (6042)
2.8		5974 (1343)	10 360 (2329)	12 686 (2852)	15 395 (3461)	16 610 (3734)	6810 (1531)	13 438 (3021)	17 357 (3902)	19 034 (4279)	28 740 (6461)
3.0		6250 (1405)	11 196 (2517)	13 812 (3105)	16 983 (3818)	21 276 (4783)	6904 (1552)	13 625 (3063)	17 637 (3965)	19 407 (4363)	30 048 (6755)
3.2		6437 (1447)	11 943 (2685)	14 741 (3314)	18 104 (4070)	24 634 (5538)		13 718 (3084)	17 824 (4007)	19 781 (4447)	31 258 (7027)
3.4		6530 (1468)	12 317 (2769)	15 302 (3440)	18 571 (4175)	27 619 (6209)		13 905 (3126)	18 011 (4049)	19 968 (4489)	32 378 (7279)
3.6			12 691 (2853)	15 675 (3524)	19 034 (4279)	29 487 (6629)		13 998 (3147)	18 104 (4070)	20 248 (4552)	33 126 (7447)
3.8			12 878 (2895)	15 956 (3587)	19 407 (4363)	31 164 (7006)		14 092 (3168)	18 198 (4091)	20 417 (4590)	33 780 (7594)
4.0			13 251 (2979)	16 143 (3629)	19 781 (4447)	32 472 (7300)		14 185 (3189)	18 384 (4133)	20 715 (4657)	34 340 (7720)
4.2			13 438 (3021)	16 236 (3650)	20 061 (4510)	33 499 (7531)		14 279 (3210)	18 473 (4153)	20 809 (4678)	34 807 (7825)
4.4			13 625 (3063)	16 423 (3692)	20 342 (4573)	34 153 (7678)		14 372 (3231)	18 571 (4175)	20 996 (4720)	35 270 (7929)
4.6				16 516 (3713)	20 435 (4594)	34 714 (7804)		14 466 (3252)	18 665 (4196)	21 089 (4741)	35 643 (8013)
4.8				16 610 (3734)	20 622 (4636)	35 270 (7929)		14 555 (3272)	18 754 (4216)	21 182 (4762)	35 924 (8076)
5.0				16 703 (3755)	20 715 (4657)	35 643 (8013)		14 648 (3293)	18 847 (4237)	21 276 (4783)	36 204 (8139)
5.2				16 796 (3776)	20 902 (4699)	36 017 (8097)		14 741 (3314)		21 463 (4825)	36 391 (8181)
5.4					20 996 (4720)	36 297 (8160)				21 556 (4846)	36 578 (8223)
5.6					21 089 (4741)	36 578 (8223)				21 649 (4867)	36 671 (8244)
5.8					21 276 (4783)	36 671 (8244)					36 764 (8265)
6.0					21 463 (4825)	36 764 (8265)					
6.2					21 556 (4846)						
6.4					21 649 (4867)						
6.6					21 930 (4930)						
6.8					22 023 (4951)						

TABLE I.- SIMULATED ENGINE RESPONSE CHARACTERISTICS — Continued

(a) Acceleration — Concluded

Time, sec	Thrust response, N (lbf), for T_c, N (lbf), of —											
	36 764 (8265)	18 198 (4091)	36 764 (8265)	13 905 (3126)	22 397 (5035)	36 764 (8265)	19 594 (4405)	22 953 (5160)	36 764 (8265)	22 953 (5160)	36 764 (8265)	36 764 (8265)
0	4 479 (1007)	11 196 (2517)	11 196 (2517)	12 317 (2769)	12 317 (2769)	12 317 (2769)	16 796 (3776)	16 796 (3776)	16 796 (3776)	20 715 (4657)	20 715 (4657)	24 447 (5496)
.2	4 853 (1091)	12 317 (2769)	12 317 (2769)	12 878 (2895)	13 998 (3147)	13 998 (3147)	18 291 (4112)	19 221 (4321)	19 221 (4321)	21 836 (4909)	24 074 (5412)	27 806 (6251)
.4	5 600 (1259)	14 555 (3272)	15 675 (3524)	13 251 (2979)	16 796 (3776)	16 796 (3776)	18 940 (4258)	20 342 (4573)	24 074 (5412)	22 116 (4972)	30 048 (6755)	31 912 (7174)
.6	7 090 (1594)	15 302 (3440)	20 528 (4615)	13 438 (3021)	18 291 (4112)	22 397 (5035)	19 127 (4300)	21 089 (4741)	27 993 (6293)	22 303 (5014)	32 472 (7300)	33 407 (7510)
.8	9 519 (2140)	16 049 (3608)	24 634 (5538)	13 531 (3042)	19 407 (4363)	26 129 (5874)	19 407 (4363)	21 836 (4909)	30 608 (6881)	22 490 (5056)	33 780 (7594)	34 528 (7762)
1.0	12 878 (2895)	16 610 (3734)	27 993 (6293)	13 625 (3063)	20 342 (4573)	29 113 (6545)	19 594 (4405)	22 397 (5035)	32 472 (7300)	22 677 (5098)	34 527 (7762)	35 644 (8013)
1.2	17 917 (4028)	17 170 (3860)	30 234 (6797)	13 718 (3084)	20 902 (4699)	30 868 (6944)		22 677 (5098)	33 593 (7552)	22 770 (5119)	35 087 (7888)	36 205 (8139)
1.4	22 397 (5035)	17 357 (3902)	31 538 (7090)	13 812 (3105)	21 463 (4825)	32 285 (7258)		22 953 (5160)	34 247 (7699)	22 953 (5160)	35 643 (8013)	36 764 (8265)
1.6	25 755 (5790)	17 637 (3965)	32 472 (7300)	13 905 (3126)	21 930 (4930)	33 219 (7468)			34 714 (7804)		36 017 (8097)	
1.8	28 553 (6419)	17 917 (4028)	33 219 (7468)		22 210 (4993)	33 966 (7636)			35 270 (7929)		36 391 (8181)	
2.0	30 421 (6839)	18 011 (4049)	33 780 (7594)		22 397 (5035)	34 527 (7762)			35 830 (8055)		36 764 (8265)	
2.2	31 444 (7069)	18 104 (4070)	34 340 (7720)			35 087 (7888)			36 204 (8139)			
2.4	32 285 (7258)	18 198 (4091)	34 714 (7804)			35 457 (7971)			36 578 (8223)			
2.6	32 846 (7384)		35 270 (7929)			35 830 (8055)			36 764 (8265)			
2.8	33 499 (7531)		35 830 (8055)			36 297 (8160)						
3.0	34 153 (7678)		36 204 (8139)			36 578 (8223)						
3.2	34 714 (7804)		36 484 (8202)			36 764 (8265)						
3.4	35 087 (7888)		36 671 (8244)									
3.6	35 457 (7971)		36 764 (8265)									
3.8	35 737 (8034)											
4.0	35 924 (8076)											
4.2	36 110 (8118)											
4.4	36 204 (8139)											
4.6	36 391 (8181)											
4.8	36 484 (8202)											
5.0	36 578 (8223)											
5.2	36 671 (8244)											
5.4	36 764 (8265)											

TABLE I.- SIMULATED ENGINE RESPONSE CHARACTERISTICS – Continued

(b) Deceleration

Time, sec	Thrust response, N (lbf), for T_c, N (lbf), of –									
	1 681 (378)	8 772 (1972)	17 357 (3902)	19 781 (4447)	24 447 (5496)	1 681 (378)	13 069 (2938)	16 796 (3776)	21 836 (4909)	1 681 (378)
0	36 764 (8265)	36 764 (8265)	36 764 (8265)	36 764 (8265)	36 764 (8265)	24 634 (5538)	24 634 (5538)	24 634 (5538)	23 513 (5286)	22 770 (5119)
.2	32 846 (7384)	32 846 (7384)	32 846 (7384)	32 846 (7384)	32 846 (7384)	21 743 (4888)	21 743 (4888)	22 210 (4993)	23 046 (5181)	20 155 (4531)
.4	26 876 (6042)	26 876 (6042)	26 876 (6042)	26 876 (6042)	26 876 (6042)	19 221 (4321)	19 221 (4321)	20 155 (4531)	22 677 (5098)	18 198 (4091)
.6	22 397 (5035)	22 397 (5035)	24 447 (5496)	24 634 (5538)	24 634 (5538)	17 170 (3860)	17 170 (3860)	19 034 (4279)	22 397 (5035)	16 049 (3608)
.8	18 847 (4237)	18 847 (4237)	22 584 (5077)	23 700 (5328)	24 447 (5496)	15 675 (3524)	15 675 (3524)	18 478 (4154)	22 210 (4993)	13 998 (3147)
1.0	16 610 (3734)	16 610 (3734)	21 463 (4825)	23 140 (5202)		14 092 (3168)	15 022 (3377)	18 104 (4070)	22 116 (4972)	12 504 (2811)
1.2	14 928 (3356)	15 302 (3440)	21 099 (4741)	22 770 (5119)		12 691 (2853)	14 555 (3272)	17 824 (4007)	21 930 (4930)	11 290 (2538)
1.4	13 812 (3105)	14 372 (3231)	20 715 (4657)	22 397 (5035)		11 196 (2517)	14 092 (3168)	17 637 (3965)	21 836 (4909)	10 449 (2349)
1.6	12 504 (2811)	13 812 (3105)	20 342 (4573)	22 210 (4993)		10 449 (2349)	13 812 (3105)	17 450 (3923)		9 706 (2182)
1.8	11 570 (2601)	13 438 (3021)	19 968 (4489)	22 023 (4951)		9 519 (2140)	13 438 (3021)	17 357 (3902)		8 959 (2014)
2.0	10 916 (2454)	12 971 (2916)	19 594 (4405)	21 836 (4909)		8 772 (1972)	13 251 (2979)	17 263 (3881)		8 398 (1888)
2.2	10 266 (2308)	12 691 (2853)	19 221 (4321)	21 649 (4867)		8 211 (1846)	13 069 (2938)	17 170 (3860)		7 838 (1762)
2.4	9 519 (2140)	12 410 (2790)	19 034 (4279)	21 463 (4825)		7 838 (1762)		17 077 (3839)		7 277 (1636)
2.6	8 772 (1972)	12 130 (2727)	18 847 (4237)	21 276 (4783)		7 371 (1657)		16 983 (3818)		6 904 (1552)
2.8	8 211 (1846)	11 943 (2685)	18 665 (4196)	21 089 (4741)		6 997 (1573)		16 890 (3797)		6 530 (1468)
3.0	7 838 (1762)	11 663 (2622)	18 478 (4154)	20 902 (4699)		6 717 (1510)		16 796 (3776)		6 161 (1385)
3.2	7 464 (1678)	11 476 (2580)	18 291 (4112)	20 809 (4678)		6 343 (1426)				5 787 (1301)
3.4	7 090 (1594)	11 290 (2538)	18 198 (4091)	20 715 (4657)		5 974 (1343)				5 600 (1259)
3.6	6 717 (1510)	11 103 (2496)	18 104 (4070)	20 528 (4615)		5 600 (1259)				5 320 (1196)
3.8	6 530 (1468)	11 009 (2475)	18 011 (4049)	20 435 (4594)		5 413 (1217)				5 133 (1154)
4.0	6 161 (1385)	10 822 (2433)	17 917 (4028)	20 342 (4573)		5 227 (1175)				4 853 (1091)
4.2	5 974 (1343)	10 636 (2391)	17 824 (4007)	20 248 (4552)		5 040 (1133)				4 573 (1028)
4.4	5 694 (1280)	10 449 (2349)	17 731 (3986)	20 155 (4531)		4 760 (1070)				4 386 (986)
4.6	5 413 (1217)	10 360 (2329)	17 637 (3965)	20 061 (4510)		4 479 (1007)				4 106 (923)
4.8	5 227 (1175)	10 266 (2308)	17 544 (3944)	19 968 (4489)		4 293 (965)				3 825 (860)
5.0	5 040 (1133)	10 080 (2266)	17 450 (3923)	19 875 (4468)		4 107 (923)				3 639 (818)
5.2	4 853 (1091)	9 986 (2245)	17 357 (3902)	19 781 (4447)		3 732 (839)				3 452 (776)
5.4	4 479 (1007)	9 893 (2224)				3 545 (797)				3 265 (734)
5.6	4 293 (965)	9 706 (2182)				3 358 (755)				3 172 (713)
5.8	4 106 (923)	9 613 (2161)				3 265 (734)				2 985 (671)
6.0	3 919 (881)	9 519 (2140)				3 078 (692)				2 798 (629)
6.2	3 732 (839)	9 426 (2119)				2 985 (671)				2 705 (608)
6.4	3 545 (797)	9 239 (2077)				2 798 (629)				2 518 (566)
6.6	3 172 (713)	9 145 (2056)				2 611 (587)				2 424 (545)
6.8	2 985 (671)	9 052 (2035)				2 424 (545)				2 237 (503)
7.0	2 798 (629)	8 959 (2014)				2 237 (503)				2 055 (462)
7.2	2 611 (587)	8 865 (1993)				2 055 (462)				1 962 (441)
7.4	2 424 (545)	8 772 (1972)				1 868 (420)				1 868 (420)
7.6	2 144 (482)					1 681 (378)				1 775 (399)
7.8	1 868 (420)									1 681 (378)
8.0	1 681 (378)									

TABLE I. - SIMULATED ENGINE RESPONSE CHARACTERISTICS – Concluded

(b) Deceleration – Concluded

Time, sec	Thrust response, N (lbf), for T_c, N (lbf), of –									
	3 732 (839)	17 917 (4028)	11 917 (2679)	1 681 (378)	7 464 (1678)	3 732 (839)	12 691 (2853)	1 681 (378)	3732 (839)	1681 (378)
0	20 155 (4531)	20 155 (4531)	18 754 (4216)	17 824 (4007)	17 824 (4007)	15 115 (3398)	13 998 (3147)	13 438 (3021)	7464 (1678)	5413 (1217)
.2	18 847 (4237)	19 034 (4279)	17 450 (3923)	16 423 (3692)	16 049 (3608)	14 372 (3231)	13 625 (3063)	12 504 (2811)	7184 (1615)	5133 (1154)
.4	17 170 (3860)	18 665 (4196)	15 862 (3566)	14 555 (3272)	14 741 (3314)	13 438 (3021)	13 345 (3000)	11 570 (2601)	6810 (1531)	4853 (1091)
.6	15 302 (3440)	18 478 (4154)	14 555 (3272)	13 158 (2958)	13 812 (3105)	12 130 (2727)	13 158 (2958)	10 636 (2391)	6437 (1447)	4573 (1028)
.8	13 438 (3021)	18 291 (4112)	13 812 (3105)	11 757 (2643)	12 878 (2895)	10 822 (2433)	12 971 (2916)	9 706 (2182)	6067 (1364)	4293 (965)
1.0	11 943 (2685)	18 104 (4070)	13 345 (3000)	10 449 (2349)	11 943 (2685)	9 706 (2182)	12 913 (2903)	8 772 (1972)	5694 (1280)	4012 (902)
1.2	10 822 (2433)	17 917 (4028)	12 971 (2916)	9 332 (2098)	11 383 (2559)	8 959 (2014)	12 878 (2895)	8 025 (1804)	5320 (1196)	3732 (839)
1.4	9 893 (2224)		12 691 (2853)	8 398 (1888)	10 822 (2433)	8 211 (1846)	12 784 (2874)	7 277 (1636)	5040 (1133)	3545 (797)
1.6	9 145 (2056)		12 504 (2811)	7 838 (1762)	10 449 (2349)	7 464 (1678)	12 726 (2861)	6 717 (1510)	4760 (1070)	3358 (755)
1.8	8 492 (1909)		12 410 (2790)	7 090 (1594)	10 080 (2266)	6 904 (1552)	12 691 (2853)	6 161 (1385)	4573 (1028)	3078 (692)
2.0	7 838 (1762)		11 917 (2679)	6 530 (1468)	9 706 (2182)	6 437 (1447)		5 787 (1301)	4293 (965)	2891 (650)
2.2	7 277 (1636)			6 067 (1364)	9 332 (2098)	5 974 (1343)		5 413 (1217)	4199 (944)	2611 (587)
2.4	6 904 (1552)			5 600 (1259)	9 145 (2056)	5 600 (1259)		5 040 (1133)	4106 (923)	2424 (545)
2.6	6 530 (1468)			5 227 (1175)	8 865 (1993)	5 413 (1217)		4 666 (1049)	4012 (902)	2237 (503)
2.8	6 161 (1385)			4 853 (1091)	8 585 (1930)	5 040 (1133)		4 293 (965)	3919 (881)	2144 (482)
3.0	5 787 (1301)			4 479 (1007)	8 398 (1888)	4 760 (1070)		4 012 (902)	3825 (860)	1962 (441)
3.2	5 413 (1217)			4 293 (965)	8 118 (1825)	4 479 (1007)		3 732 (839)	3732 (839)	1868 (420)
3.4	5 133 (1154)			3 919 (881)	7 838 (1762)	4 293 (965)		3 452 (776)		1775 (399)
3.6	4 853 (1091)			3 732 (839)	7 650 (1720)	4 106 (923)		3 172 (713)		1681 (378)
3.8	4 666 (1049)			3 545 (797)	7 557 (1699)	3 919 (881)		2 985 (671)		
4.0	4 386 (986)			3 265 (734)	7 464 (1678)	3 732 (839)		2 798 (629)		
4.2	4 106 (923)			2 985 (671)				2 611 (587)		
4.4	3 919 (881)			2 798 (629)				2 424 (545)		
4.6	3 732 (839)			2 611 (587)				2 237 (503)		
4.8				2 518 (566)				2 055 (462)		
5.0				2 331 (524)				1 868 (420)		
5.2				2 237 (503)				1 775 (399)		
5.4				2 055 (462)				1 681 (378)		
5.6				1 868 (420)						
5.8				1 775 (399)						
6.0				1 681 (378)						

TABLE II.- MASS AND DIMENSIONAL CHARACTERISTICS
OF SIMULATED AIRCRAFT

Weight, N (lbf) 245 097 (55 100)

Wing area, m^2 (ft^2) 78 (843)

Wing span, m (ft) 24 (78)

Mean aerodynamic chord, m (ft) 3.58 (11.74)

Center-of-gravity location, percent $\bar{c}$ 40

I_X, kg-m^2 (slug-ft^2) 331 106 (244 212)

I_Y, kg-m^2 (slug-ft^2) 334 641 (246 819)

I_Z, kg-m^2 (slug-ft^2) 625 685 (461 482)

I_{XZ}, kg-m^2 (slug-ft^2) 27 689 (20 423)

Maximum control-surface deflections:

δ_t, deg . . . . ±10

δ_{f3}, deg . . . . 0 to 90

δ_{sp}, deg . . . . 0 to 60

δ_s, deg . . . . ±60

δ_a, deg . . . . ±20

δ_r, deg . . . . ±40

Maximum control-surface deflection rates:

$\dot{\delta}_t$, deg/sec 50

$\dot{\delta}_{f3}$, deg/sec 5

$\dot{\delta}_{sp}$, deg/sec 50

$\dot{\delta}_s$, deg/sec 50

$\dot{\delta}_a$, deg/sec 50

$\dot{\delta}_r$, deg/sec 50

TABLE III. - BASIC AERODYNAMIC INPUTS USED IN SIMULATION

α, deg	c_X C_T=0	c_X C_T=1.87	c_X C_T=3.74	c_Z C_T=0	c_Z C_T=1.87	c_Z C_T=3.74	c_m C_T=0	c_m C_T=1.87	c_m C_T=3.74	$c_{X_{\delta_{T3}}}$ C_T=0	$c_{X_{\delta_{T3}}}$ C_T=1.87	$c_{X_{\delta_{T3}}}$ C_T=3.74	$c_{Z_{\delta_{T3}}}$ C_T=0	$c_{Z_{\delta_{T3}}}$ C_T=1.87	$c_{Z_{\delta_{T3}}}$ C_T=3.74	$c_{m_{\delta_{T3}}}$ C_T=0	$c_{m_{\delta_{T3}}}$ C_T=1.87	$c_{m_{\delta_{T3}}}$ C_T=3.74	c_{m_q} C_T=0	c_{m_q} C_T=1.87	c_{m_q} C_T=3.74	$c_{m_{\dot{\alpha}}}$ C_T=0	$c_{m_{\dot{\alpha}}}$ C_T=1.87	$c_{m_{\dot{\alpha}}}$ C_T=3.74
	c_X			c_Z			c_m			$c_{X_{\delta_{T3}}}$, per deg			$c_{Z_{\delta_{T3}}}$, per deg			$c_{m_{\delta_{T3}}}$, per deg			c_{m_q}, per rad			$c_{m_{\dot{\alpha}}}$, per rad		
-10	-0.330	-0.211	0.383	-0.145	-3.212	-4.739	0.80	0.25	-0.50	-0.0038	-0.0460	-0.0760	-0.0180	-0.0550	-0.0400	-0.0001	0.0016	-0.0036	-28.60	-17.86	-28.60	-11.40	-7.14	-11.40
-5	-.366	-.232	.285	-.741	-3.794	-5.345	.45	.10	-.50	-.0033	-.0435	-.0736	-.0134	-.0580	-.0610	.0006	.0021	-.0023	-28.60	-26.80	-28.60	-11.40	-10.70	-11.40
0	-.340	-.250	.300	-1.400	-4.500	-6.130	.12	-.07	-.53	-.0026	-.0403	-.0700	-.0086	-.0611	-.0861	.0013	.0026	-.0010	-28.60	-32.15	-29.30	-11.40	-12.85	-11.70
5	-.249	-.119	.432	-2.090	-5.180	-6.889	-.14	-.25	-.60	-.0029	-.0388	-.0690	-.0089	-.0593	-.0832	.0019	.0022	0	-26.45	-34.30	-30.00	-10.55	-13.70	-12.00
10	-.094	.095	.594	-2.518	-5.781	-7.572	-.23	-.37	-.68	-.0040	-.0371	-.0674	-.0040	-.0534	-.0784	.0019	.0034	.0003	-21.44	-32.86	-30.36	-8.56	-13.14	-12.14
15	.017	.344	.932	-2.770	-6.306	-8.116	-.27	-.45	-.78	-.0041	-.0360	-.0649	.0009	-.0490	-.0759	.0033	.0030	.0005	-10.72	-30.72	-31.45	-4.28	-12.28	-12.55
20	.019	.632	1.162	-2.851	-6.708	-8.601	-.27	-.50	-.84	-.0051	-.0350	-.0627	.0054	-.0492	-.0737	.0026	.0020	-.0005	-3.57	-30.00	-31.45	-1.43	-12.00	-12.55
25	.078	.864	1.535	-2.700	-7.033	-8.972	-.30	-.49	-.83	-.0046	-.0320	-.0591	.0040	-.0455	-.0734	.0030	.0016	-.0004	-5.00	-28.60	-30.36	-2.00	-11.40	-12.14
30	.111	.798	1.765	-2.592	-5.602	-9.258	-.32	-.40	-.75	-.0055	-.0099	-.0514	.0060	-.0527	-.0683	.0022	.0042	-.0006	-9.29	-39.30	-48.60	-3.71	-15.70	-19.40

α, deg	$c_{X_{\delta_s}}$ C_T=0	C_T=1.87	C_T=3.74	$c_{Z_{\delta_s}}$ C_T=0	C_T=1.87	C_T=3.74	$c_{m_{\delta_s}}$ C_T=0	C_T=1.87	C_T=3.74	$c_{Y_{\delta_s}}$ C_T=0	C_T=1.87	C_T=3.74	$c_{n_{\delta_s}}$ C_T=0	C_T=1.87	C_T=3.74	$c_{l_{\delta_s}}$ C_T=0	C_T=1.87	C_T=3.74	c_{Y_p} C_T=0	C_T=1.87	C_T=3.74	c_{n_p} C_T=0	C_T=1.87	C_T=3.74
	$c_{X_{\delta_s}}$, per deg			$c_{Z_{\delta_s}}$, per deg			$c_{m_{\delta_s}}$, per deg			$c_{Y_{\delta_s}}$, per deg			$c_{n_{\delta_s}}$, per deg			$c_{l_{\delta_s}}$, per deg			c_{Y_p}, per rad			c_{n_p}, per rad		
-10	-0.0012	-0.0024	-0.0026	0.0093	0.0140	0.0148	-0.0012	0.0006	0.0052	-0.0002	0	0.0002	0.0007	0.0007	0.0005	0.0015	0.0023	0.0024	-0.02	-0.09	-0.49	-0.15	-0.11	0.38
-5	-.0016	-.0016	-.0028	.0105	.0165	.0161	-.0017	-.0007	.0025	-.0002	-.0001	.0002	.0008	.0008	.0009	.0020	.0029	.0028	-.04	-.04	-.10	-.04	-.15	-.12
0	-.0020	-.0008	-.0030	.0117	.0192	.0173	-.0022	-.0020	-.0002	-.0002	-.0002	0	.0009	.0009	.0013	.0025	.0035	.0032	0	.05	.11	-.02	-.22	-.30
5	-.0026	-.0013	-.0032	.0128	.0209	.0173	-.0008	-.0022	-.0017	-.0002	-.0002	-.0001	.0009	.0010	.0015	.0027	.0038	.0033	.07	.19	.10	-.20	-.28	-.25
10	-.0033	-.0021	-.0028	.0119	.0217	.0185	-.0002	-.0020	-.0020	-.0003	-.0003	-.0002	.0009	.0011	.0015	.0026	.0038	.0032	.05	.25	.53	-.16	-.33	-.40
15	-.0035	-.0033	-.0046	.0099	.0219	.0186	.0008	-.0012	-.0012	-.0002	-.0003	-.0002	.0009	.0011	.0015	.0022	.0036	.0031	.24	.45	.80	-.20	-.45	-.52
20	-.0028	-.0037	-.0033	.0078	.0210	.0176	.0013	-.0008	-.0005	-.0002	-.0003	-.0002	.0008	.0011	.0014	.0017	.0035	.0029	.30	.80	1.20	-.22	-.50	-.57
25	-.0017	-.0032	-.0048	.0036	.0209	.0163	.0017	-.0008	-.0002	-.0002	-.0004	-.0002	.0008	.0010	.0013	.0011	.0037	.0028	.06	.89	1.25	-.15	-.40	-.59
30	0	-.0068	-.0029	.0015	.0117	.0160	.0020	-.0012	-.0005	-.0002	-.0004	-.0003	.0007	.0010	.0012	.0008	.0038	.0028	.13	.75	1.03	-.14	-.22	-.15

α, deg	$c_{X_{\delta_t}}$ C_T=0	C_T=1.87	C_T=3.74	$c_{Z_{\delta_t}}$ C_T=0	C_T=1.87	C_T=3.74	$c_{m_{\delta_t}}$ C_T=0	C_T=1.87	C_T=3.74	$c_{Y_{\delta_r}}$ C_T=0	C_T=1.87	C_T=3.74	$c_{n_{\delta_r}}$ C_T=0	C_T=1.87	C_T=3.74	$c_{l_{\delta_r}}$ C_T=0	C_T=1.87	C_T=3.74	c_{l_p} C_T=0	C_T=1.87	C_T=3.74	c_{Y_r} C_T=0	C_T=1.87	C_T=3.74
	$c_{X_{\delta_t}}$, per deg			$c_{Z_{\delta_t}}$, per deg			$c_{m_{\delta_t}}$, per deg			$c_{Y_{\delta_r}}$, per deg			$c_{n_{\delta_r}}$, per deg			$c_{l_{\delta_r}}$, per deg			c_{l_p}, per rad			c_{Y_r}, per rad		
-10	-0.0092	0.0072	-0.0049	-0.0242	-0.0160	-0.0102	-0.090	-0.084	-0.028	0.012	0.010	0.009	-0.0043	-0.0051	-0.0046	0.0020	0.0016	0.0019	-0.05	-1.13	-0.78	0.76	0.88	0.94
-5	-.0062	.0042	-.0019	-.0246	-.0204	-.0101	-.085	-.087	-.044	.012	.010	.009	-.0041	-.0047	-.0046	.0018	.0016	.0020	-.60	-.88	-.75	.76	.86	.92
0	-.0030	.0010	.0010	-.0250	-.0250	-.0100	-.080	-.090	-.060	.012	.010	.009	-.0039	-.0043	-.0046	.0016	.0016	.0021	-.98	-.68	-.72	.77	.90	1.00
5	-.0002	-.0012	.0004	-.0201	-.0202	-.0050	-.065	-.097	-.076	.011	.010	.009	-.0038	-.0041	-.0046	.0016	.0017	.0022	-.68	-.50	-.68	.77	1.03	1.20
10	-.0036	-.0044	-.0070	-.0138	-.0211	-.0174	-.040	-.092	-.088	.010	.010	.009	-.0036	-.0040	-.0046	.0016	.0017	.0022	-.40	-.50	-.63	.78	1.08	1.60
15	-.0018	-.0071	-.0015	-.0088	-.0122	-.0252	-.013	-.078	-.098	.010	.010	.010	-.0034	-.0040	-.0046	.0011	.0017	.0022	-.37	-.50	-.55	.80	1.00	1.35
20	-.0006	-.0011	.0002	-.0042	-.0057	-.0180	.002	-.069	-.089	.009	.011	.010	-.0024	-.0040	-.0046	.0003	.0016	.0020	-.32	-.33	-.42	.59	.70	1.24
25	-.0042	-.0051	-.0030	-.0053	-.0079	-.0124	.002	-.060	-.080	.006	.012	.012	-.0020	-.0041	-.0047	-.0003	.0010	.0017	-.26	-.17	-.33	.33	.32	.93
30	-.0002	-.0152	.0339	-.0036	-.0312	-.0728	-.005	-.050	-.079	.002	.010	.012	-.0002	-.0033	-.0042	.0006	.0008	.0014	-.26	-.08	-.25	-.08	1.70	2.55

α, deg	c_{Y_β} C_T=0	C_T=1.87	C_T=3.74	c_{n_β} C_T=0	C_T=1.87	C_T=3.74	c_{l_β} C_T=0	C_T=1.87	C_T=3.74	$c_{X_{\delta_{sp}}}$ C_T=0	C_T=1.87	C_T=3.74	$c_{Z_{\delta_{sp}}}$ C_T=0	C_T=1.87	C_T=3.74	$c_{m_{\delta_{sp}}}$ C_T=0	C_T=1.87	C_T=3.74	c_{n_r} C_T=0	C_T=1.87	C_T=3.74	c_{l_r} C_T=0	C_T=1.87	C_T=3.74
	c_{Y_β}, per deg			c_{n_β}, per deg			c_{l_β}, per deg			$c_{X_{\delta_{sp}}}$, per deg			$c_{Z_{\delta_{sp}}}$, per deg			$c_{m_{\delta_{sp}}}$, per deg			c_{n_r}, per rad			c_{l_r}, per rad		
-10	-0.020	-0.022	-0.050	0.0030	0.0035	0.0053	0.0012	0	0	0	-0.0060	-0.0044	0.0260	0.0430	0.0300	-0.006	0	0.008	-0.45	-0.33	-0.37	0.32	0.57	0.55
-5	-.020	-.050	-.050	.0038	.0052	.0070	-.0006	-.0020	-.0020	-.0016	-.0043	-.0042	.0272	.0425	.0325	-.004	0	.005	-.35	-.38	-.42	.48	.70	.77
0	-.020	-.050	-.055	.0042	.0078	.0081	-.0024	-.0036	-.0031	-.0040	-.0010	-.0040	.0290	.0420	.0380	-.002	0	.002	-.30	-.42	-.45	.67	.80	.86
5	-.020	-.050	-.055	.0043	.0082	.0086	-.0034	-.0048	-.0044	-.0048	-.0018	-.0056	.0317	.0440	.0417	0	0	.001	-.33	-.41	-.45	.77	.85	.85
10	-.020	-.050	-.055	.0043	.0080	.0081	-.0023	-.0051	-.0053	-.0052	-.0016	-.0045	.0296	.0434	.0429	.001	0	.001	-.34	-.42	-.54	.83	.80	.80
15	-.023	-.050	-.055	.0047	.0082	.0089	-.0028	-.0051	-.0061	-.0046	-.0012	-.0080	.0247	.0432	.0414	.004	.001	.002	-.38	-.42	-.52	.88	.82	.83
20	-.024	-.050	-.055	.0050	.0084	.0092	-.0029	-.0062	-.0066	-.0036	-.0046	-.0070	.0157	.0420	.0387	.005	.001	.002	-.35	-.40	-.52	.73	.90	.90
25	-.020	-.050	-.055	.0021	.0083	.0088	-.0070	-.0067	-.0072	.0001	-.0025	-.0085	.0045	.0408	.0347	.004	.001	.003	-.30	-.34	-.47	.83	1.10	.93
30	-.024	-.020	-.055	.0018	-.0040	.0082	-.0050	-.0070	-.0090	.0012	-.0082	-.0024	.0019	-.0022	.0321	.004	.001	.003	-.20	-.42	-.70	.62	-.20	-.50

TABLE III.- BASIC AERODYNAMIC INPUTS USED IN SIMULATION – Concluded

$\alpha,$ deg	$C_T=0$	$C_T=0.70$	$C_T=1.40$	$C_T=2.10$	$C_T=2.81$	$C_T=0$	$C_T=0.70$	$C_T=1.40$	$C_T=2.10$	$C_T=2.81$	$C_T=0$	$C_T=0.70$	$C_T=1.40$	$C_T=2.10$	$C_T=2.81$
	$C_{Y_{\delta_a}}$, per deg					$C_{n_{\delta_a}}$, per deg					$C_{l_{\delta_a}}$, per deg				
-10	-0.0016	-0.0010	-0.0004	0.0002	0.0008	-0.0014	-0.0028	-0.0040	-0.0052	-0.0064	0.0082	0.0083	0.0084	0.0085	0.0086
-5	-.0012	-.0007	-.0002	.0003	.0008	-.0001	-.0017	-.0032	-.0047	-.0062	.0048	.0058	.0068	.0078	.0088
0	-.0008	-.0004	0	.0004	.0008	.0012	-.0006	-.0024	-.0042	-.0060	.0014	.0033	.0052	.0071	.0090
5	-.0004	-.0002	0	.0002	.0004	-.0010	-.0022	-.0034	-.0046	-.0058	.0014	.0033	.0052	.0071	.0090
10	-.0006	-.0004	-.0002	0	.0002	-.0010	-.0022	-.0034	-.0046	-.0058	.0010	.0030	.0050	.0070	.0090
15	-.0008	-.0006	-.0004	-.0002	.0001	.0004	-.0011	-.0026	-.0041	-.0056	.0027	.0044	.0061	.0078	.0096
20	-.0022	-.0018	-.0014	-.0010	-.0005	.0045	.0026	.0007	-.0012	-.0032	.0207	.0197	.0187	.0177	.0168
25	-.0036	-.0024	-.0012	0	-.0012	.0036	.0024	.0010	-.0002	-.0014	-.0010	.0050	.0110	.0170	.0240
30	-.0007	-.0006	-.0005	-.0004	-.0003	.0024	.0008	-.0008	-.0024	-.0040	-.0076	-.0012	.0052	.0116	.0180

TABLE IV.- PERFORMANCE LIMITS FOR EACH INDEPENDENT
DEGREE OF FREEDOM

Degree of freedom	Performance limits				
	Position		Velocity		Acceleration
Longitudinal	Fore	1.244 m (4.08 ft)	±0.610 m/sec	(2.00 ft/sec)	±0.6g
	Aft	1.219 m (4.00 ft)			
Lateral	Left	1.219 m (4.00 ft)	±0.610 m/sec	(2.00 ft/sec)	±0.6g
	Right	1.219 m (4.00 ft)			
Vertical	Up	0.991 m (3.25 ft)	±0.610 m/sec	(2.00 ft/sec)	±0.8g
	Down	0.762 m (2.50 ft)			
Yaw	±32 deg		±15 deg/sec		±50 deg/sec^2
Pitch	±30 deg		±15 deg/sec		±50 deg/sec^2
	−20 deg				
Roll	±22 deg		±15 deg/sec		±50 deg/sec^2

TABLE V.- WASHOUT-PARAMETER VALUES USED IN SIMULATION[a]

Variable	Value in SI Units	Program value	Variable	Value in SI Units	Program value
$k_{z,1}$	0.2	0.2	B_1, sec	0.15	0.15
$\xi_{z,1}$	0.7	0.7	B_2, sec	0.15	0.15
$\omega_{n,z,1}$, rad/sec	0.1	0.1	B_3, sec	0.133	0.133
$k_{z,2}$	1.0	1.0	$k_{\psi,l}$, sec	0.15	0.15
$k_{p,T,1}$, per m (per ft)	0.013	0.004	$k_{\theta,l}$, sec	0.15	0.15
$k_{p,T,2}$, sec	3.8	3.8	$k_{\phi,l}$, sec	0.15	0.15
$k_{p,T,3}$, per sec	0.05	0.05	k_p	0.5	0.5
$k_{q,T,1}$, per m (per ft)	0.013	0.004	k_q	1.0	1.0
$k_{q,T,2}$, sec	3.8	3.8	k_r	1.0	1.0
$k_{q,T,3}$, per sec	0.05	0.05	C_1, per sec	0.5	0.5
$k_{r,1}$, per m (per ft)	0.0131	0.004	C_2, per sec	0.2	0.2
$k_{r,2}$, sec	3.8	3.8	C_3, per sec	0.5	0.5
$k_{r,3}$, per sec	0.05	0.05	$k_{\theta,1}$	1.0	1.0
a_1, rad/sec	1.414	1.414	$k_{\theta,2}$	0.04	0.04
a_2, rad/sec	2.1	2.1	ξ_θ	0.028	0.028
a_3, rad/sec	2.1	2.1	$\omega_{n,\theta}$, rad/sec	1.0	1.0
b_1, rad/sec	1.0	1.0	$k_{\phi,1}$	0.5	0.5
b_2, rad/sec	2.25	2.25	$k_{\phi,2}$	0.04	0.04
b_3, rad/sec	2.25	2.25	ξ_ϕ	0.028	0.028
$\ddot{x}_l$, m/sec^2 (ft/sec^2)	5.8840	19.3044	$\omega_{n,\phi}$, rad/sec	1.0	1.0
$\ddot{y}_l$, m/sec^2 (ft/sec^2)	5.8840	19.3044	z_{neut}, m (ft)	0.6487	2.128
$\ddot{z}_l$, m/sec^2 (ft/sec^2)	7.8453	25.7392	V_l, m/sec (ft/sec)	0.3048	1.0
A_1, sec^2	0.007	0.007	x_{LF}	2.5	2.5
A_2, sec^2	0.007	0.007	y_{LF}	2.5	2.5
A_3, sec^2	0.007	0.007	z_{LF}	3.0	3.0

[a]Washout parameters are defined in reference 7.

TABLE VI.- CHARACTERISTICS OF SIMULATOR CONTROL SYSTEM

Control	Maximum travel in −			Breakout force		Force gradient	
	deg	cm	in.	N	lbf	N/cm	lbf/in.
Column:							
Forward	6.9	9.75	3.84	4.7	1.07	12.1	6.9
Aft	11.9	14.71	5.79				
Wheel	±17.6	±20.57	±8.10	11.1	2.5	5.3	3.0
Pedel	24.8			0	0	38.0	21.7

TABLE VII.- PREFILTER AND FEEDBACK GAIN MATRICES   G   AND   F

FOR DECOUPLED LATERAL AND LONGITUDINAL CONTROLS

(a) Lateral mode

ω_R = 2.298 rad/sec; ζ_R = 0.80; P_R = 4.54 sec; $(t_{1/2})_R$ = 0.38 sec

$$G = \begin{bmatrix} -7.734535 & 1.588237 & 0.0 \\ 6.267414 & 0.714128 & 0.0 \\ 13.962874 & -1.067195 & 0.0 \end{bmatrix}$$

$$F = \begin{bmatrix} 0.868495 & 6.990785 & -21.222495 & 0.122524 \\ 0.273273 & 2.615730 & -2.238758 & -0.116009 \\ -0.374135 & -1.615966 & 33.748233 & -0.522822 \end{bmatrix}$$

(b) Longitudinal mode

ω_{sp} = 5.36 rad/sec; ζ_{sp} = 0.79; P_{sp} = 1.93 sec; $(t_{1/2})_{sp}$ = 0.16 sec

$$G = \begin{bmatrix} 1.479356 & 3.424809 & 0.882762 & 0.0 \\ 2.638624 & 0.319423 & -7.582873 & 0.0 \\ 12.143196 & -4.229370 & -8.572163 & 0.0 \\ -11.227652 & 0.079126 & 6.239296 & 0.0 \end{bmatrix}$$

$$F = \begin{bmatrix} 1.615774 & -0.397886 & -2.006868 & 3.845354 \\ -4.873305 & -16.546972 & -2.428593 & 0.368500 \\ 5.489366 & -0.247396 & -13.759019 & -2.883877 \\ -2.592946 & 2.912773 & 6.699955 & -2.834244 \end{bmatrix}$$

TABLE VIII.- TOUCHDOWN CONDITIONS FOR FIXED-BASE SIMULATOR AND MOVING-BASE SIMULATOR WITHOUT MOTION

[Pitch angle was maintained at zero throughout flights
by decoupled longitudinal controls]

(a) Fixed-base simulator (table XII of ref. 6)

Turbulence level	$\mu_{\dot{h}}$, m/sec (ft/sec)	$\sigma_{\dot{h}}$, m/sec (ft/sec)	μ_x, m (ft)	σ_x, m (ft)	No. of tests	No. of tests outside desired landing area	
						Short	Long
$\sigma_g < 0.61$ m/sec (2 ft/sec)	1.19 (3.9)	0.55 (1.8)	156.5 (513.6)	61.8 (202.7)	42	0	10
$\sigma_g \geqq 0.61$ m/sec (2 ft/sec)	1.34 (4.4)	0.61 (2.0)	147.4 (483.4)	57.8 (189.7)	31	2	7

(b) Moving-base simulator in fixed-base mode

Turbulence level	$\mu_{\dot{h}}$, m/sec (ft/sec)	$\sigma_{\dot{h}}$, m/sec (ft/sec)	μ_x, m (ft)	σ_x, m (ft)	No. of tests	No. of tests outside desired landing area	
						Short	Long
$\sigma_g < 0.61$ m/sec (2 ft/sec)	0.88 (2.9)	0.34 (1.1)	148.7 (488.0)	41.2 (135.1)	13	0	0
$\sigma_g \geqq 0.61$ m/sec (2 ft/sec)	1.01 (3.3)	0.67 (2.2)	152.8 (501.2)	73.8 (242.1)	14	2	2

TABLE IX. - PILOT RATING SYSTEM

CONTROLLABLE Capable of being controlled or managed in context of mission, with available pilot attention.	ACCEPTABLE May have deficiencies which warrant improvement, but adequate for mission. Pilot compensation, if required to achieve acceptable performance, is feasible.	SATISFACTORY Meets all requirements and expectations; good enough without improvement. Clearly adequate for mission.	Excellent, highly desirable.	1
			Good, pleasant, well behaved.	2
			Fair. Some mildly unpleasant characteristics. Good enough for mission without improvement.	3
		UNSATISFACTORY Reluctantly acceptable. Deficiencies which warrant improvement. Performance adequate for mission with feasible pilot compensation.	Some minor but annoying deficiencies. Improvement is requested. Effect on performance is easily compensated for by pilot.	4
			Moderately objectionable deficiencies. Improvement is needed. Reasonable performance requires considerable pilot compensation.	5
			Very objectionable deficiencies. Major improvements are needed. Requires best available pilot compensation to achieve acceptable performance.	6
	UNACCEPTABLE Deficiencies which require improvement. Inadequate performance for mission even with maximum feasible pilot compensation.		Major deficiencies which require improvement for acceptance. Controllable. Performance inadequate for mission, or pilot compensation required for minimum acceptable performance in mission is too high.	7
			Controllable with difficulty. Requires substantial pilot skill and attention to retain control and continue mission.	8
			Marginally controllable in mission. Requires maximum available pilot skill and attention to retain control.	9
UNCONTROLLABLE Control will be lost during some portion of mission.			Uncontrollable in mission.	10

TABLE X.- TOUCHDOWN CONDITIONS WITH DECOUPLED CONTROLS

Turbulence level	$\mu_{\dot{h}}$, m/sec (ft/sec)	$\sigma_{\dot{h}}$, m/sec (ft/sec)	μ_x, m (ft)	σ_x, m (ft)	No. of tests	No. of tests outside desired landing area	
						Short	Long
$\sigma_g < 0.61$ m/sec (2 ft/sec)	0.70 (2.3)	0.40 (1.3)	157.4 (516.3)	35.8 (117.3)	13	0	1
$\sigma_g \geq 0.61$ m/sec (2 ft/sec)	1.19 (3.9)	0.55 (1.8)	150.6 (494.1)	68.0 (223.0)	17	0	3

TABLE XI.- PREFILTER AND FEEDBACK GAIN MATRICES G AND F

FOR DECOUPLED LONGITUDINAL CONTROLS WITH

REDUCED RESPONSE TO TURBULENCE

$\omega_{sp} = 4.678$ rad/sec; $\zeta_{sp} = 0.71$; $P_{sp} = 1.92$ sec; $(t_{1/2})_{sp} = 0.21$ sec

$\omega_{ph} = 0.903$ rad/sec; $\zeta_{ph} = 0.91$; $P_{ph} = 17.14$ sec; $(t_{1/2})_{ph} = 0.84$ sec

$$G = \begin{bmatrix} 2.776885 & 1.645801 & -0.092977 & 0.0 \\ 0.599393 & -0.059215 & -5.880013 & 0.0 \\ 1.467427 & -3.211352 & -0.755450 & 0.0 \\ -3.867356 & 0.988445 & 0.868685 & 0.0 \end{bmatrix}$$

$$F = \begin{bmatrix} 0.528169 & -0.020643 & -0.656279 & 2.942620 \\ -5.253016 & -14.399142 & -0.307930 & 0.016808 \\ 1.458376 & 2.065692 & -0.881299 & -1.037223 \\ -2.066648 & -1.156426 & 2.089220 & -1.015081 \end{bmatrix}$$

TABLE XII. - TOUCHDOWN CONDITIONS WITH DECOUPLED CONTROLS AND

PREFILTER AND FEEDBACK GAINS ALTERED TO

MINIMIZE TURBULENCE EFFECTS

Turbulence level	$\mu_{\dot{h}}$, m/sec (ft/sec)	$\sigma_{\dot{h}}$, m/sec (ft/sec)	μ_x, m (ft)	σ_x, m (ft)	No. of tests	No. of tests outside desired landing area	
						Short	Long
$\sigma_g < 0.61$ m/sec (2 ft/sec)	0.67 (2.2)	0.55 (1.8)	140.0 (459.3)	52.1 (171.0)	12	0	2
$\sigma_g \geqq 0.61$ m/sec (2 ft/sec)	0.85 (2.8)	0.55 (1.8)	155.1 (509.0)	64.7 (212.3)	30	0	4
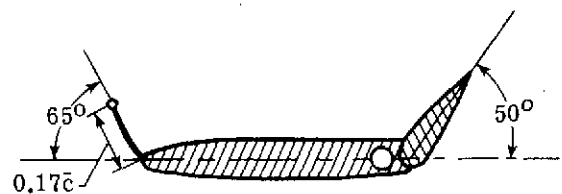
Cross section of horizontal tail
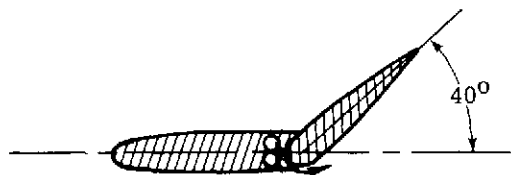
Cross section of vertical tail
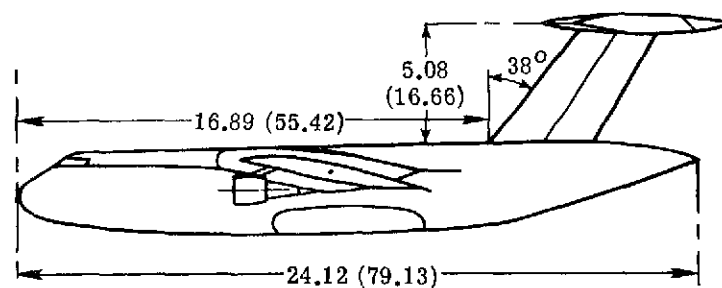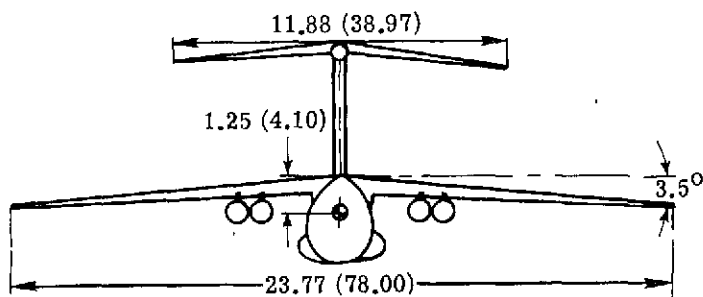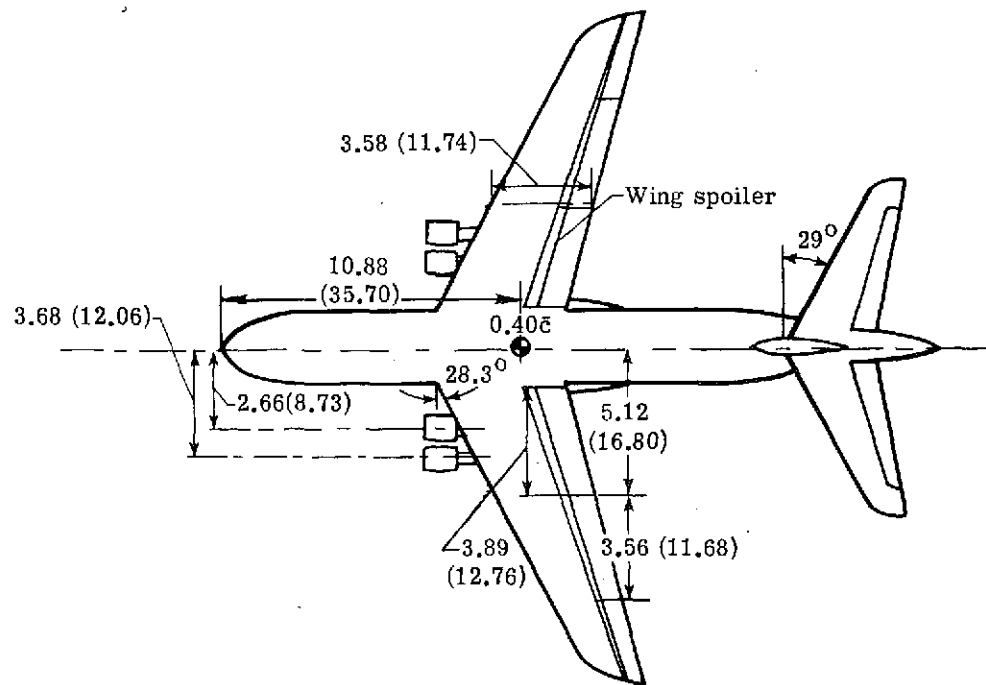
Figure 1.- Three-view drawing of simulated airplane.   All linear dimensions are in meters   (ft).
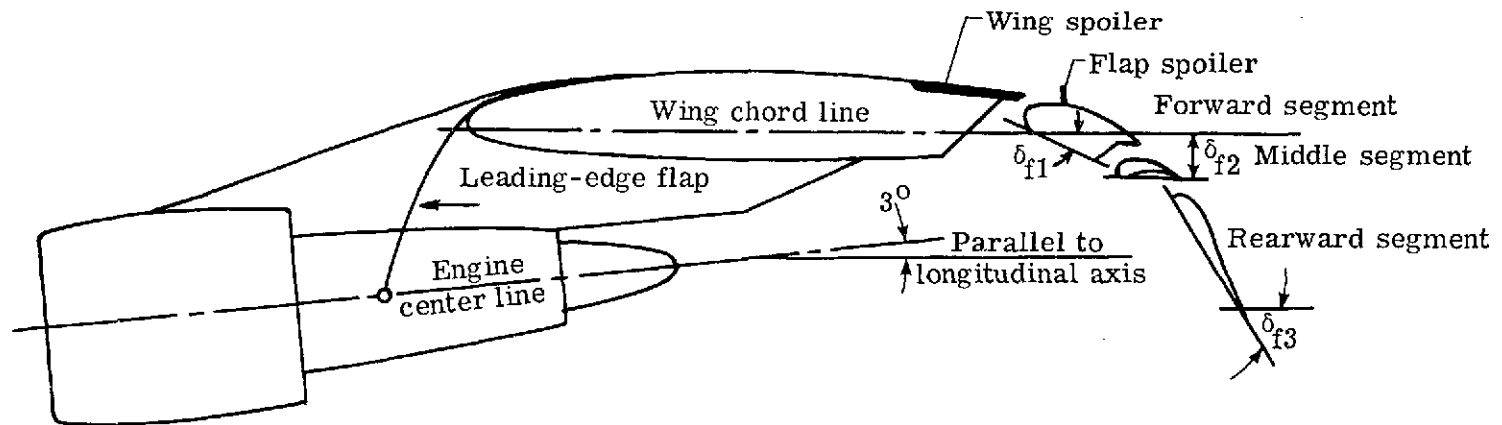
Figure 2.- Flap assembly and engine pylon detail. $\delta_{f1} = 25^\circ$; $\delta_{f2} = 10^\circ$; $\delta_{f3} = 60^\circ$.
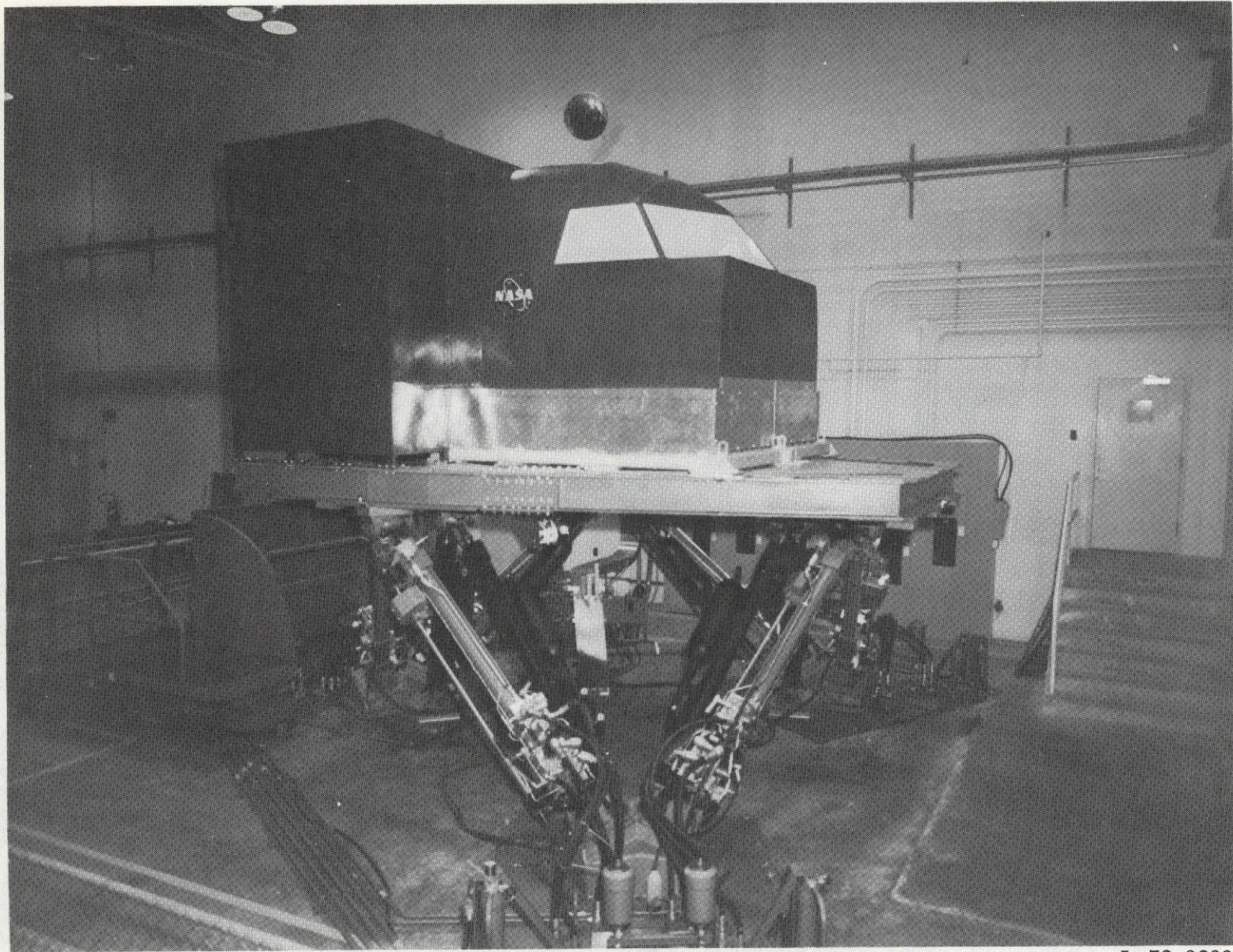
L-72-3233

Figure 3.- Moving-base simulator.
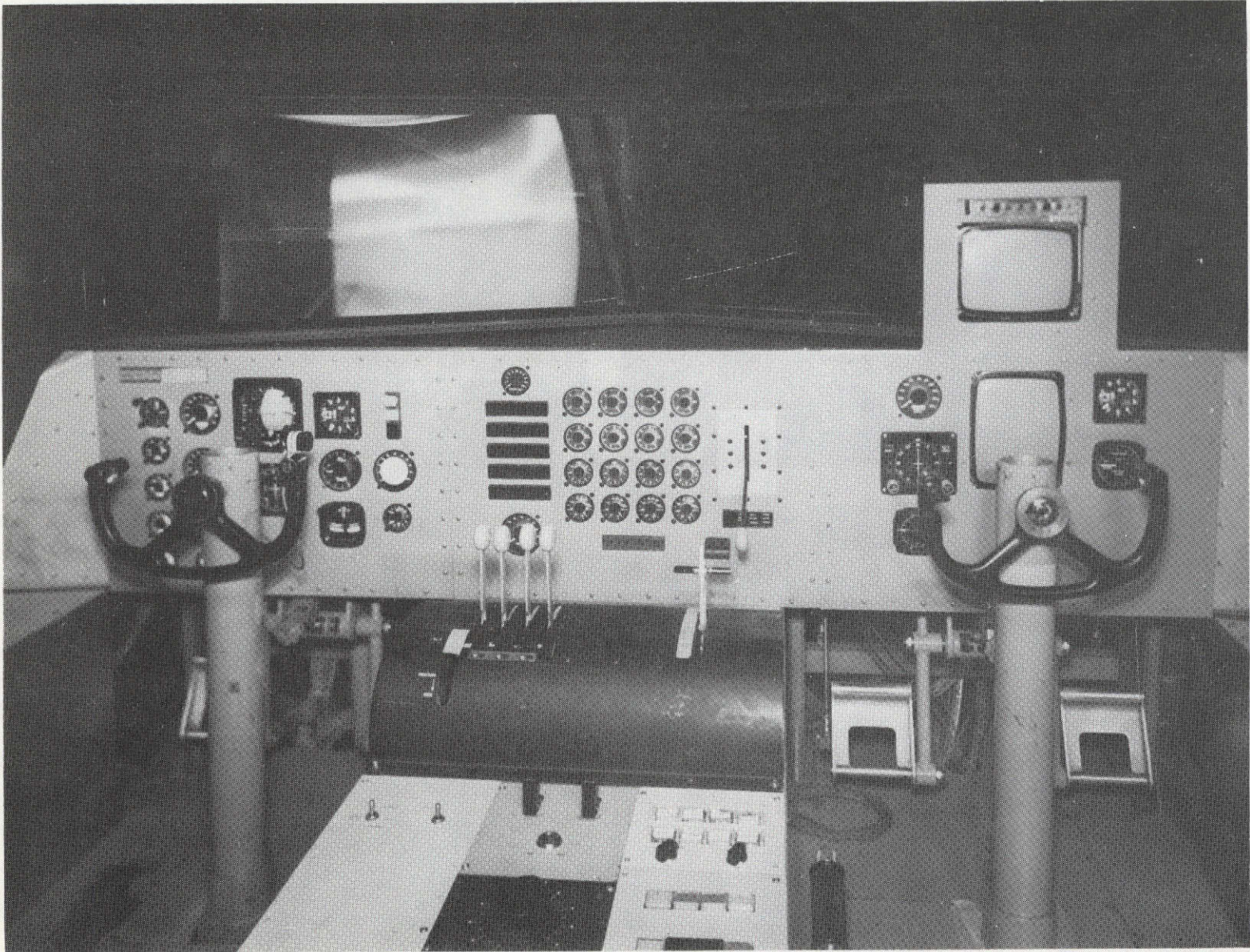
Figure 4.- Simulator cockpit.

L-73-7164

L-71-4272

Figure 5.- Photograph of 1/300-scale STOLport model.

⊠ Glide—slope transmitter

61 m
(200 ft)

45.7 m
(150 ft)

76.2 m
(250 ft)

Touchdown zone
137.2 m
(450 ft)
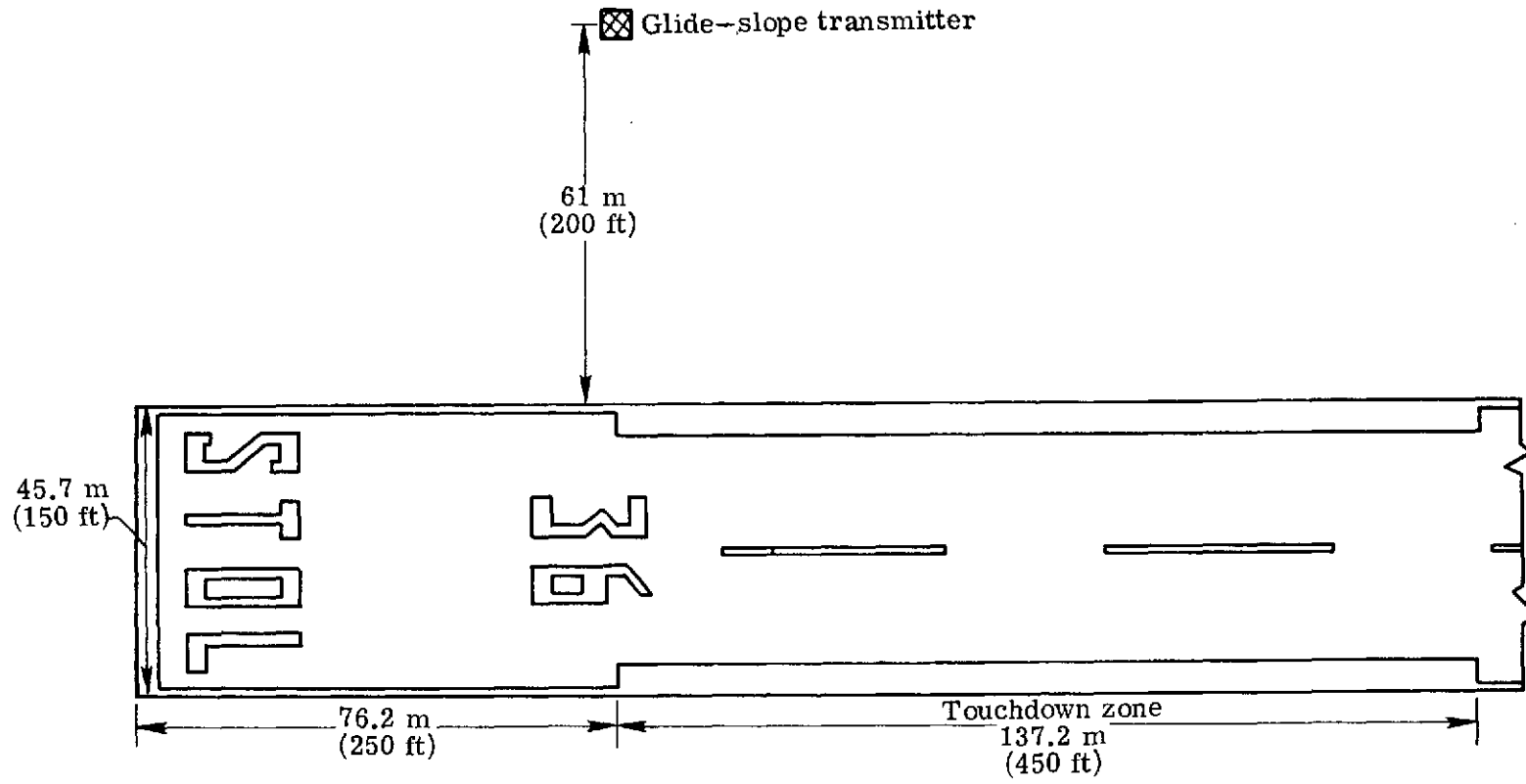
Figure 6.- Sketch of approach end of simulated runway.
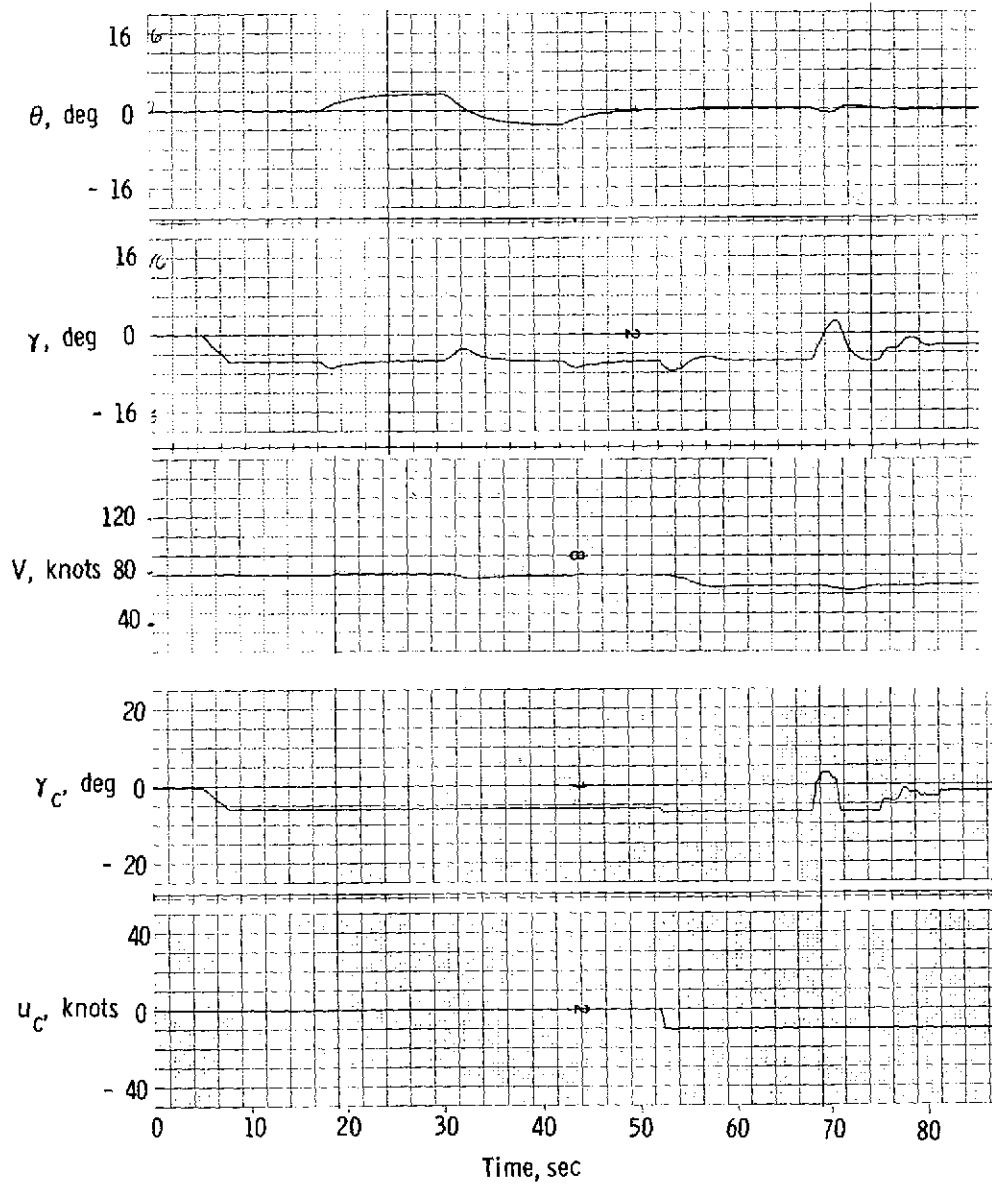
Figure 7.- Response characteristics of decoupled longitudinal controls.
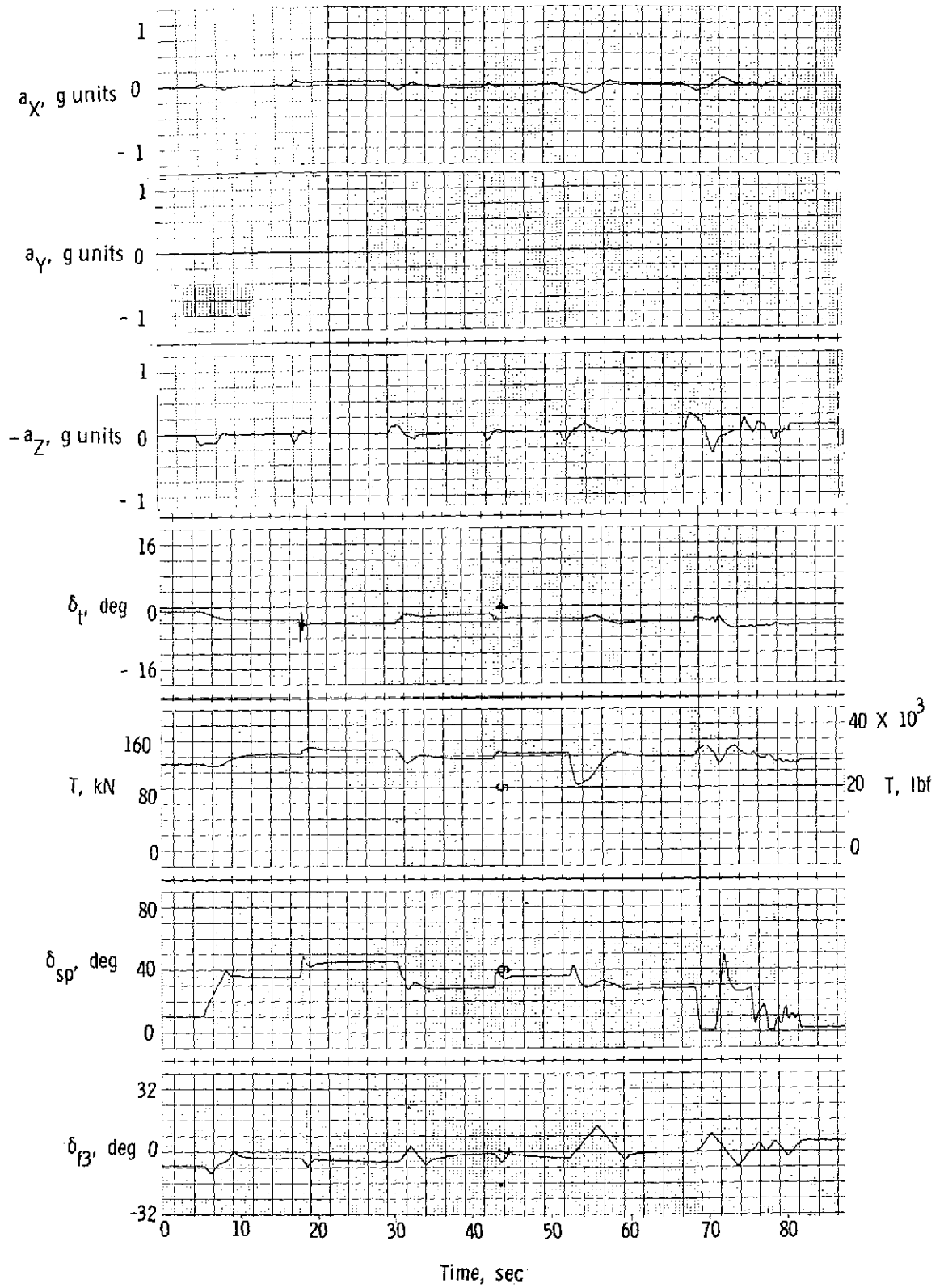
Figure 7.- Concluded.
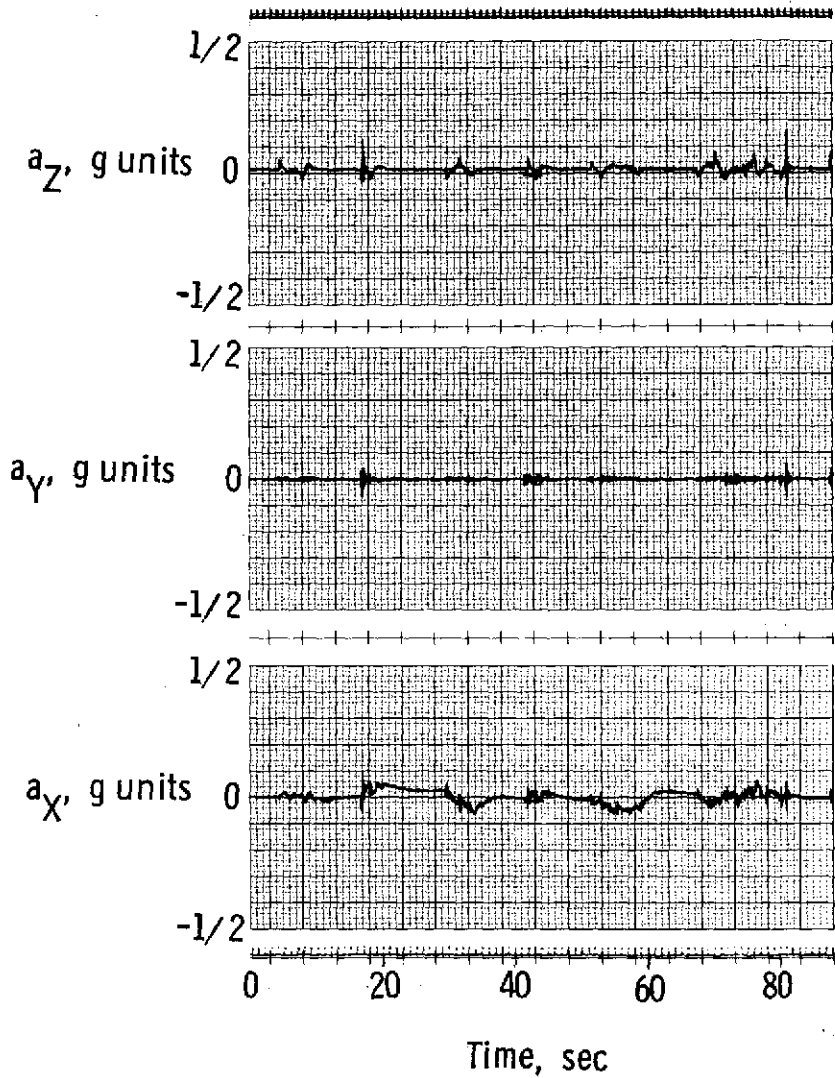
Figure 8.- Accelerometer records for response characteristics of
decoupled longitudinal controls.
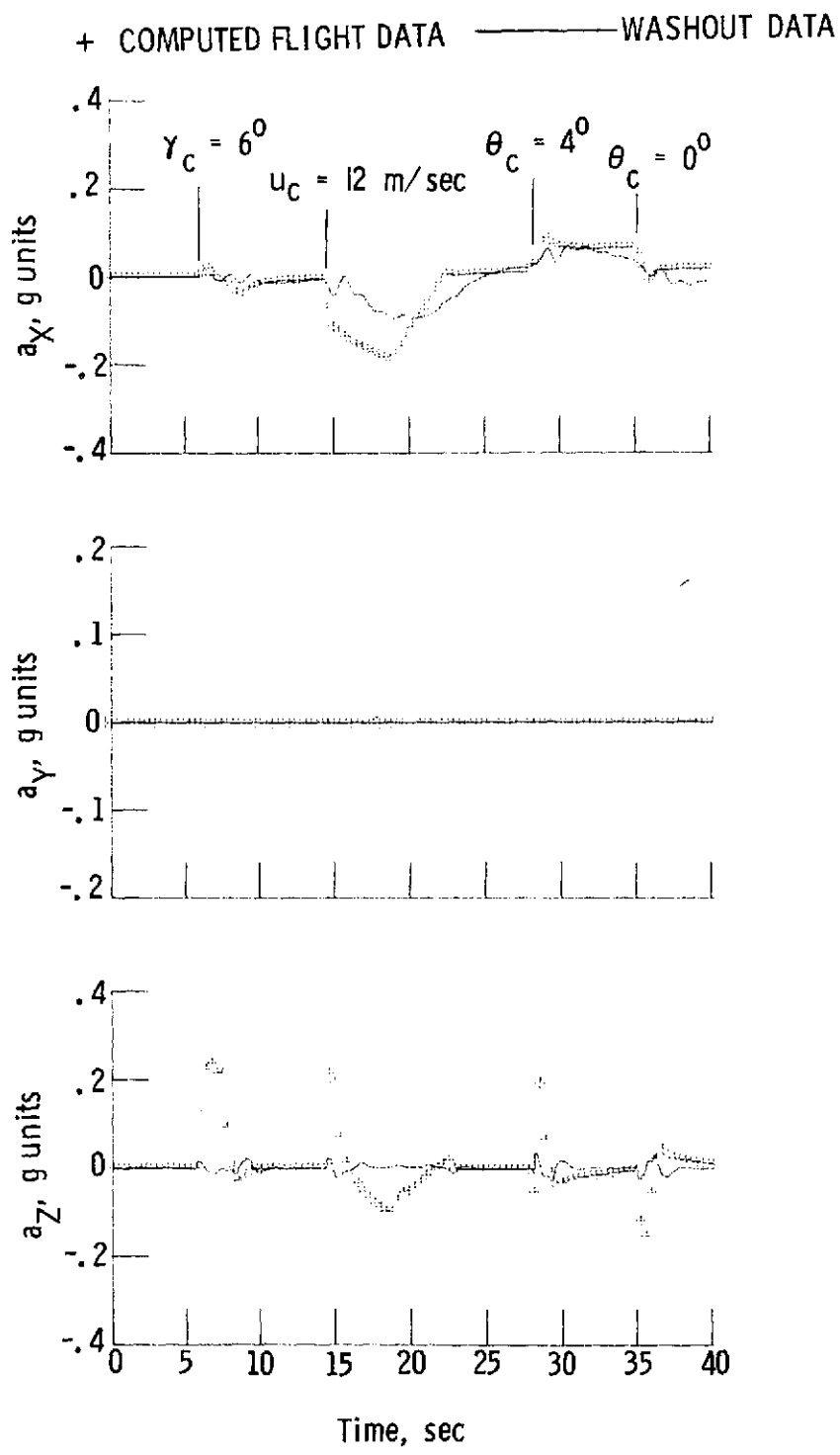
Figure 9.- Computed acceleration profiles for a typical series of control inputs before and after application of washout logic.

+COMPUTED FLIGHT DATA   ————WASHOUT DATA

Figure 9.- Continued.

Figure 9.- Continued.

Figure 9.- Concluded.
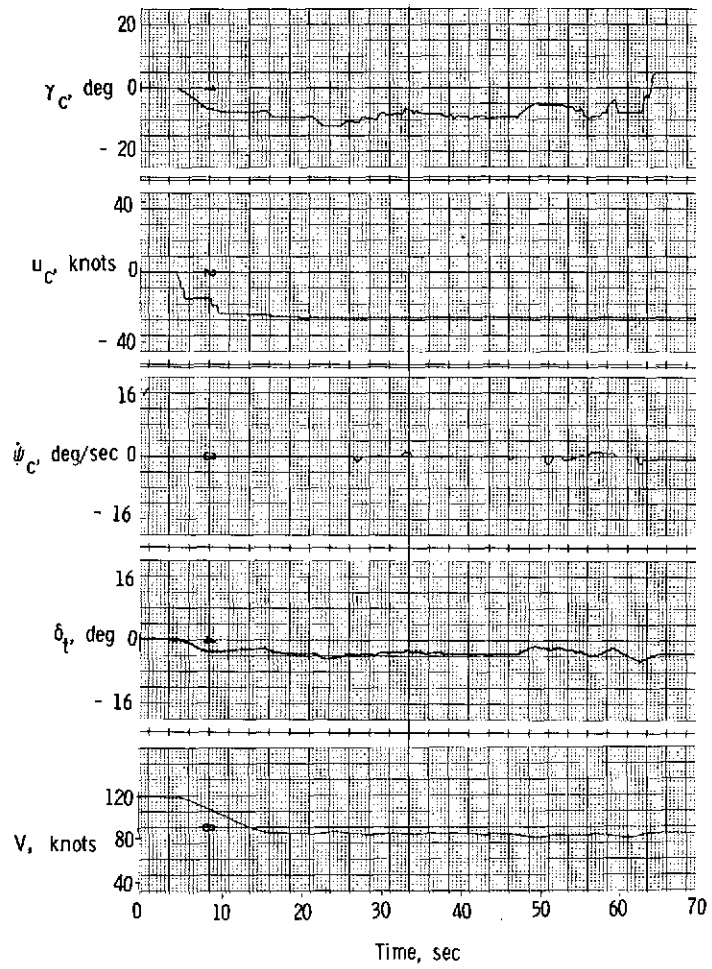
Figure 10.- Typical decelerating approach in low-level turbulence.
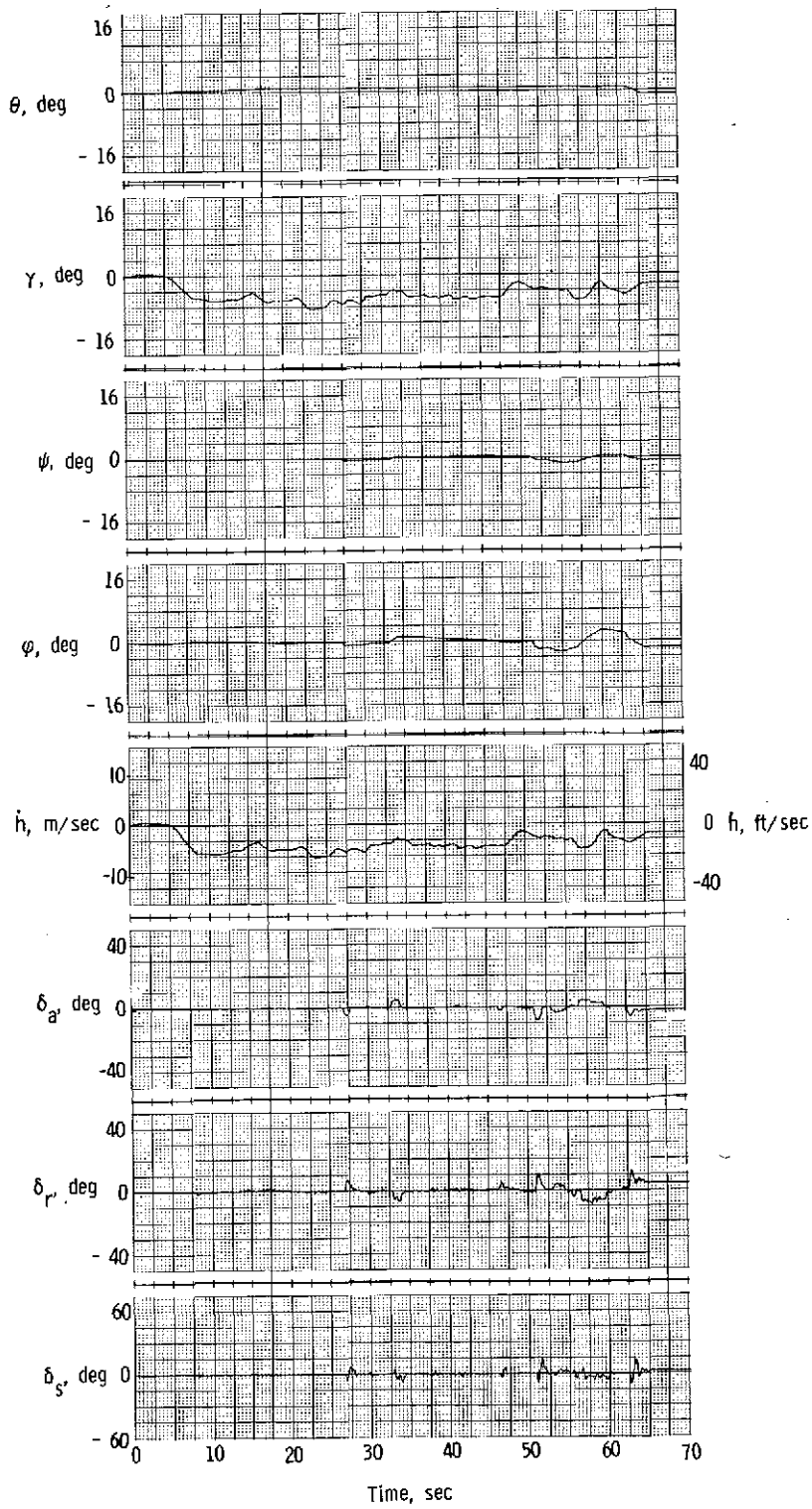
Figure 10.- Continued.
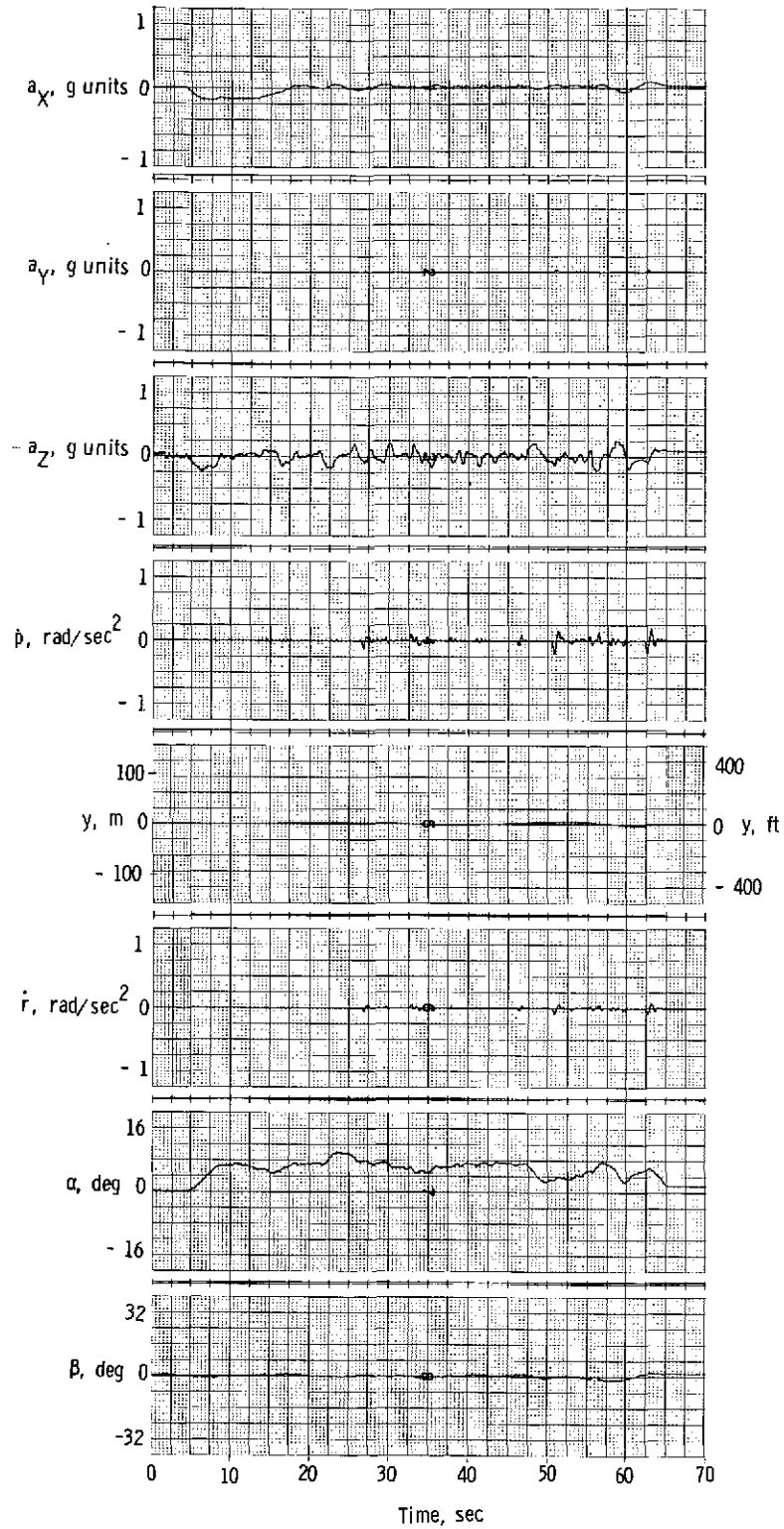
Figure 10.- Concluded.
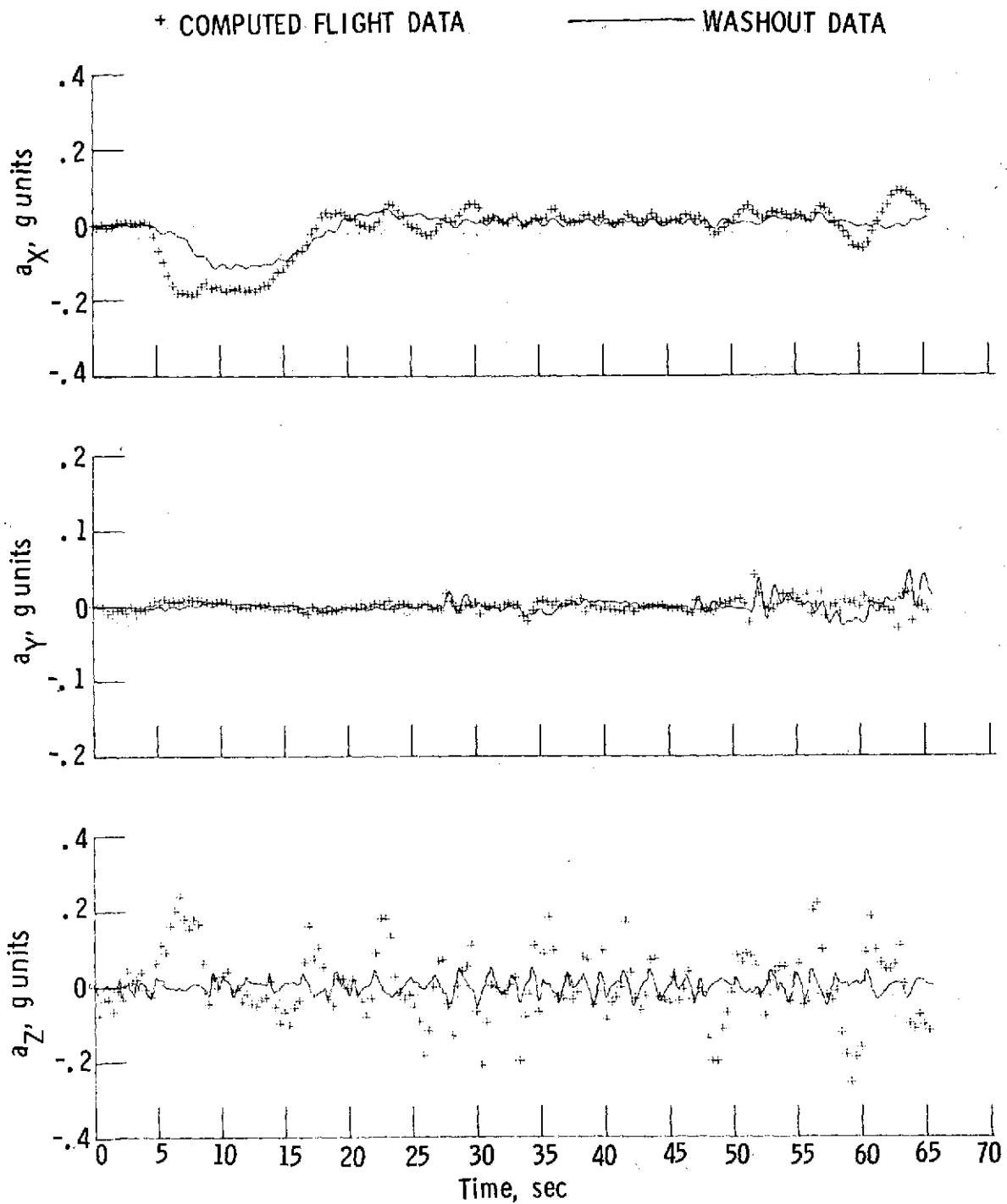
Figure 11.- Computed motion-base response for typical decelerating approach in low-level turbulence.

Figure 11.- Continued.
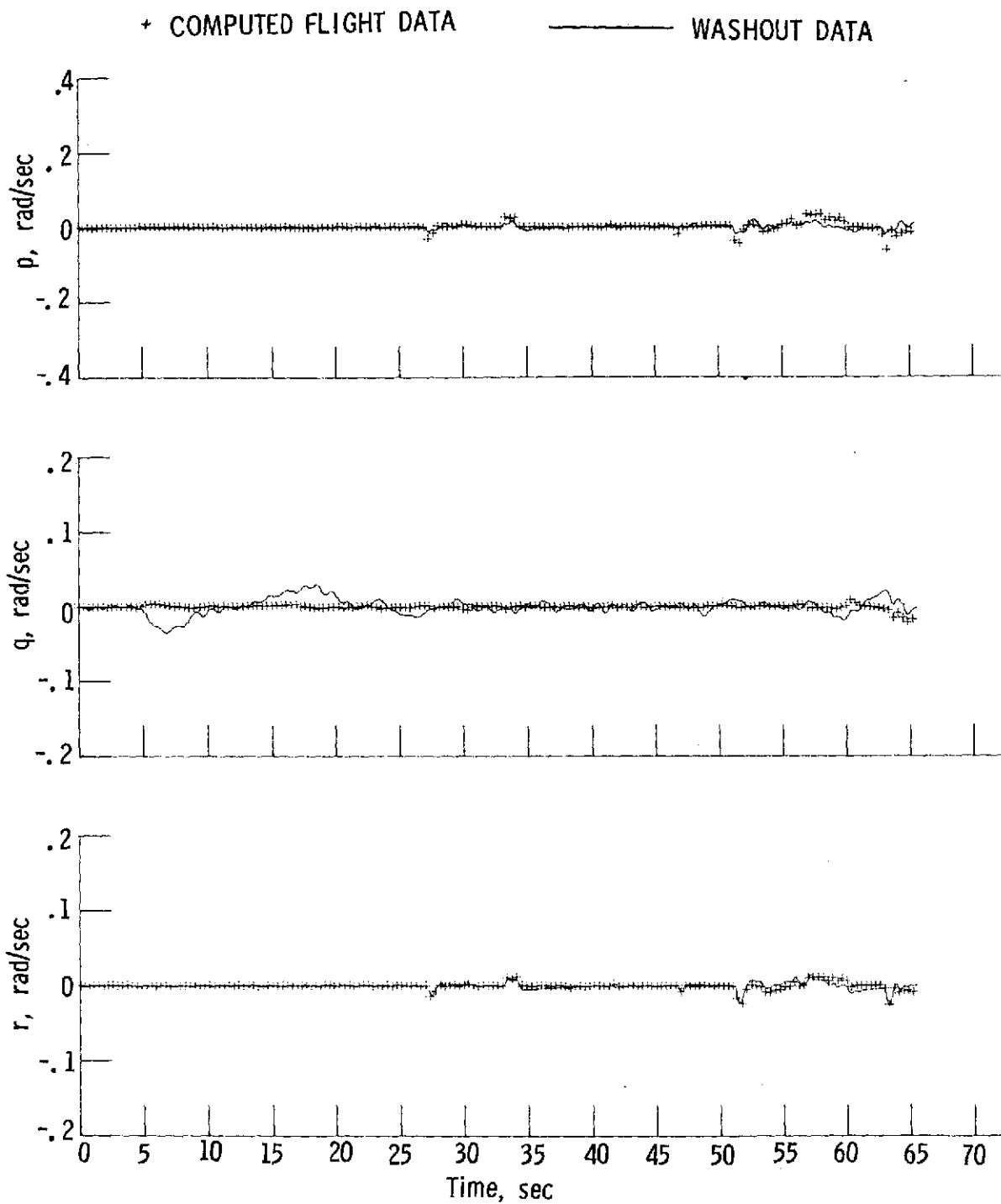
Figure 11.- Continued.

COMPUTED FLIGHT DATA ⎯⎯⎯⎯ BASE RESPONSE
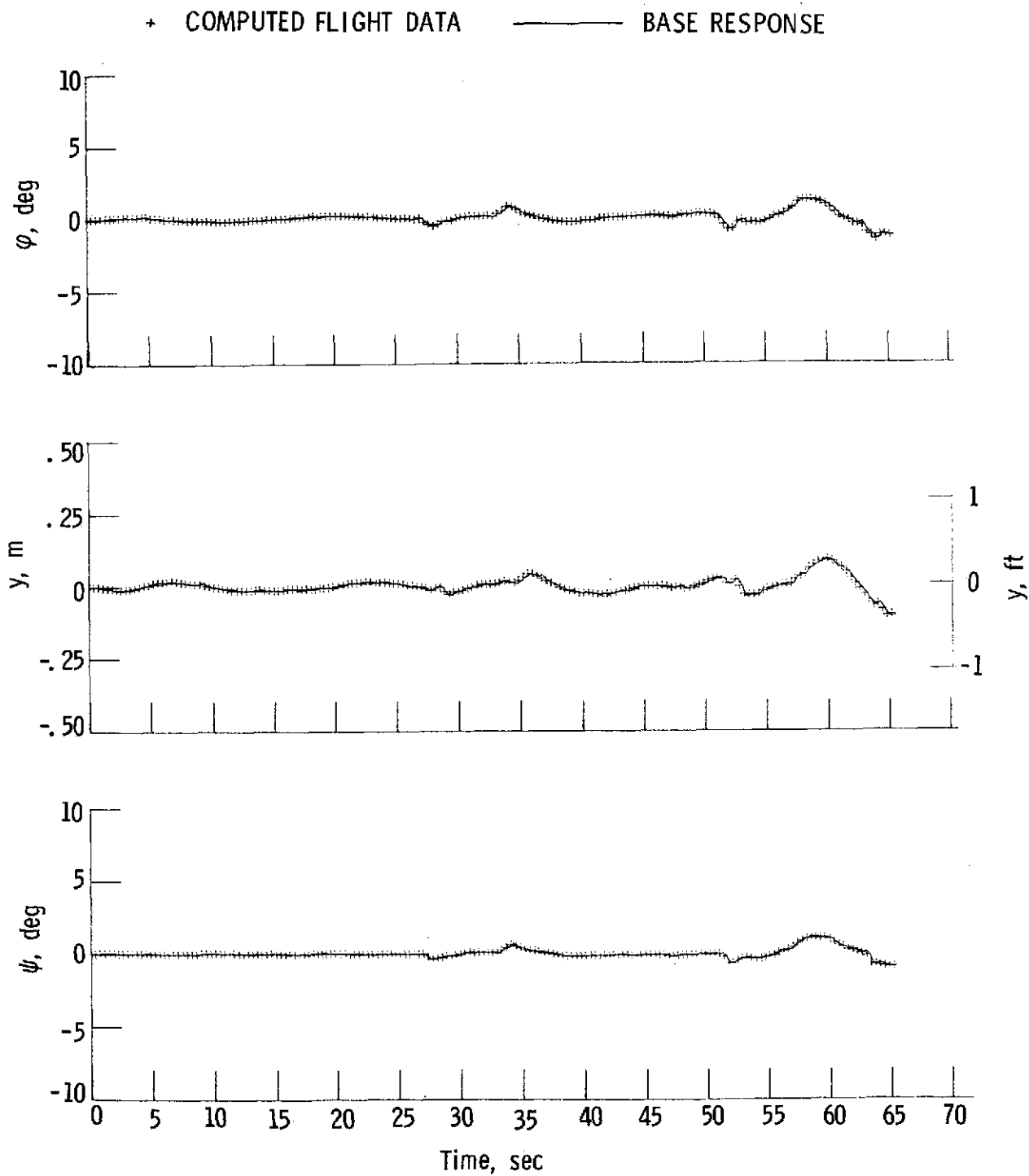
Figure 11. - Concluded.
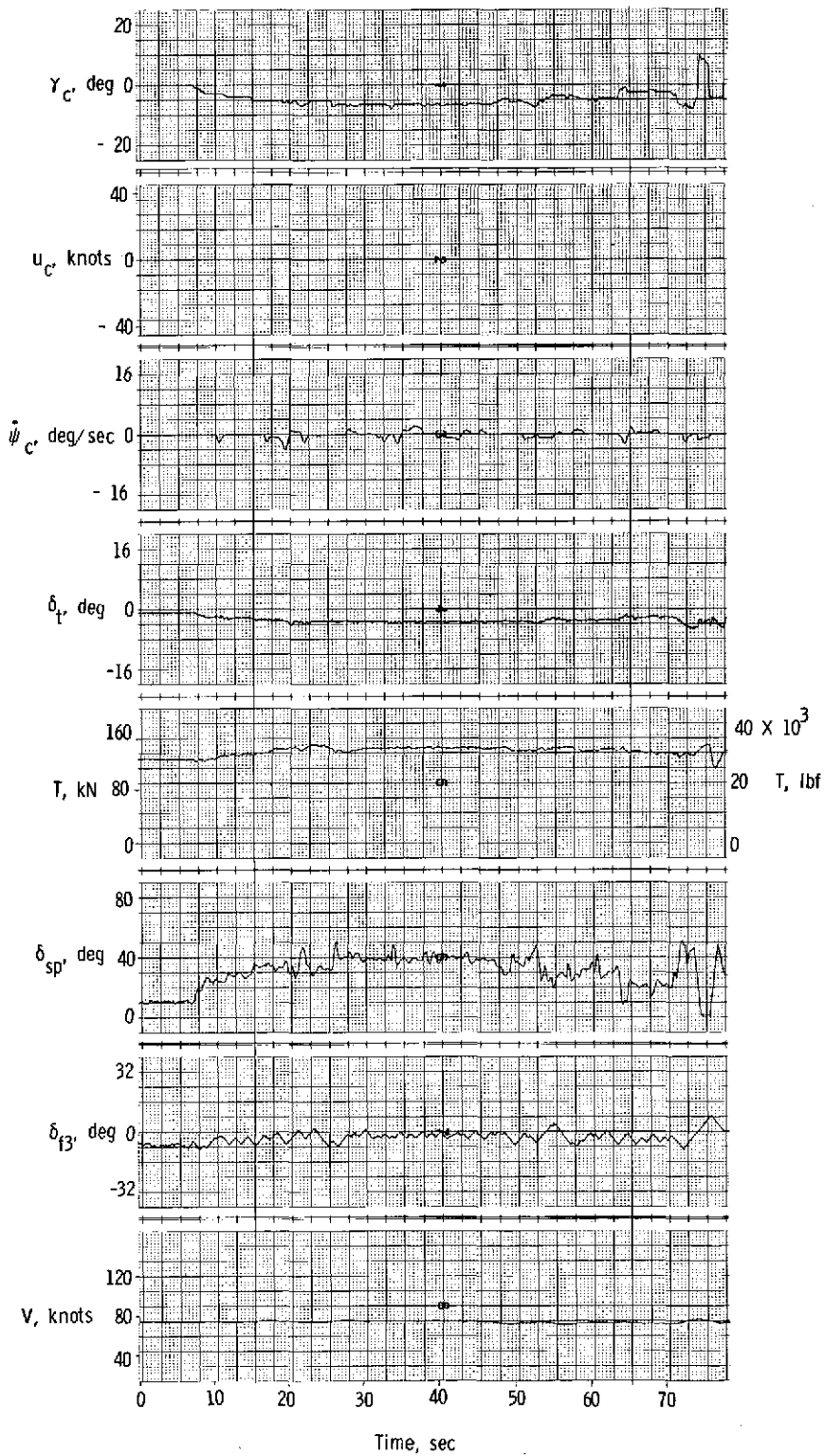
Figure 12. - Typical constant-speed two-segment approach
in low-level turbulence.
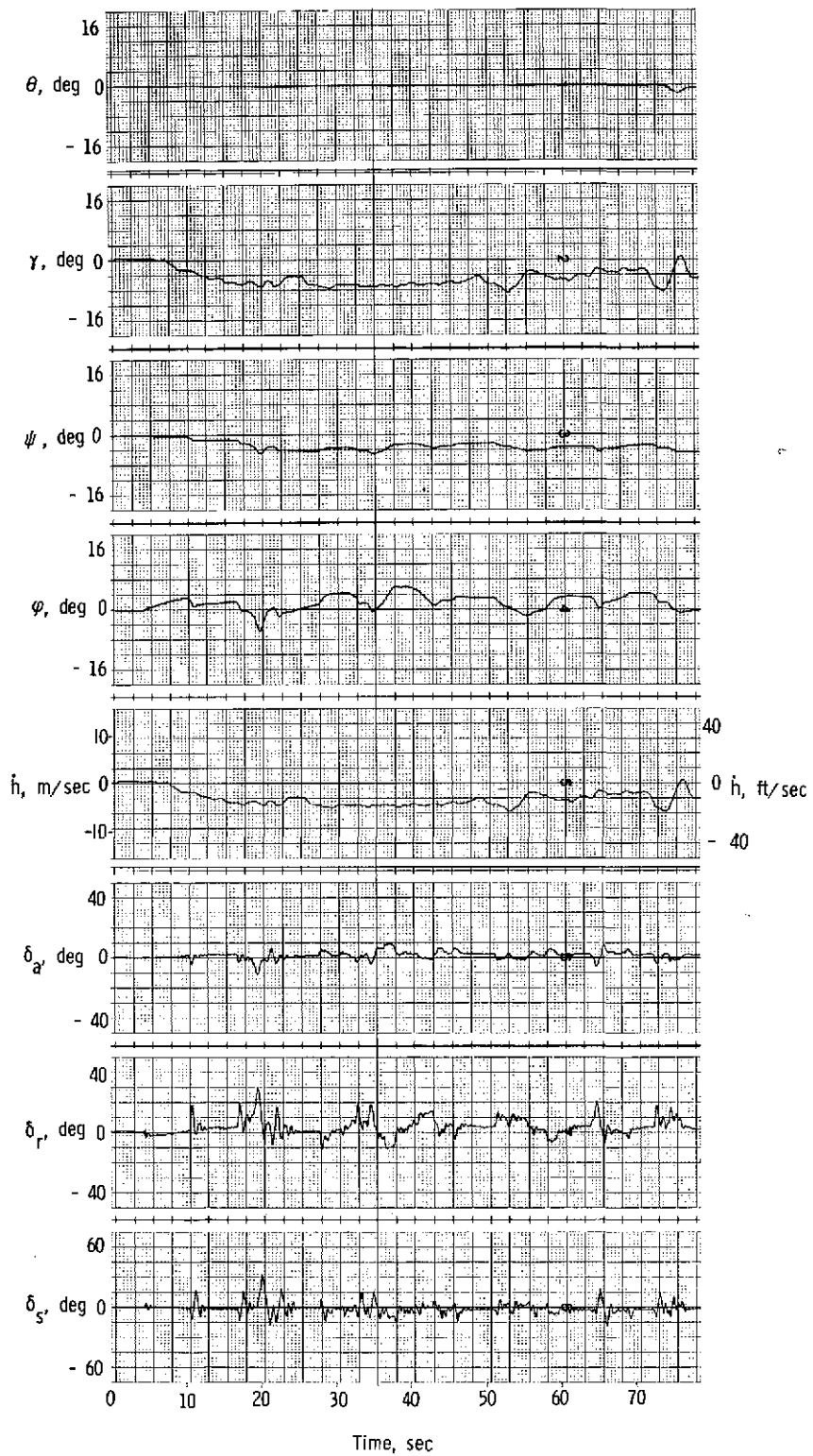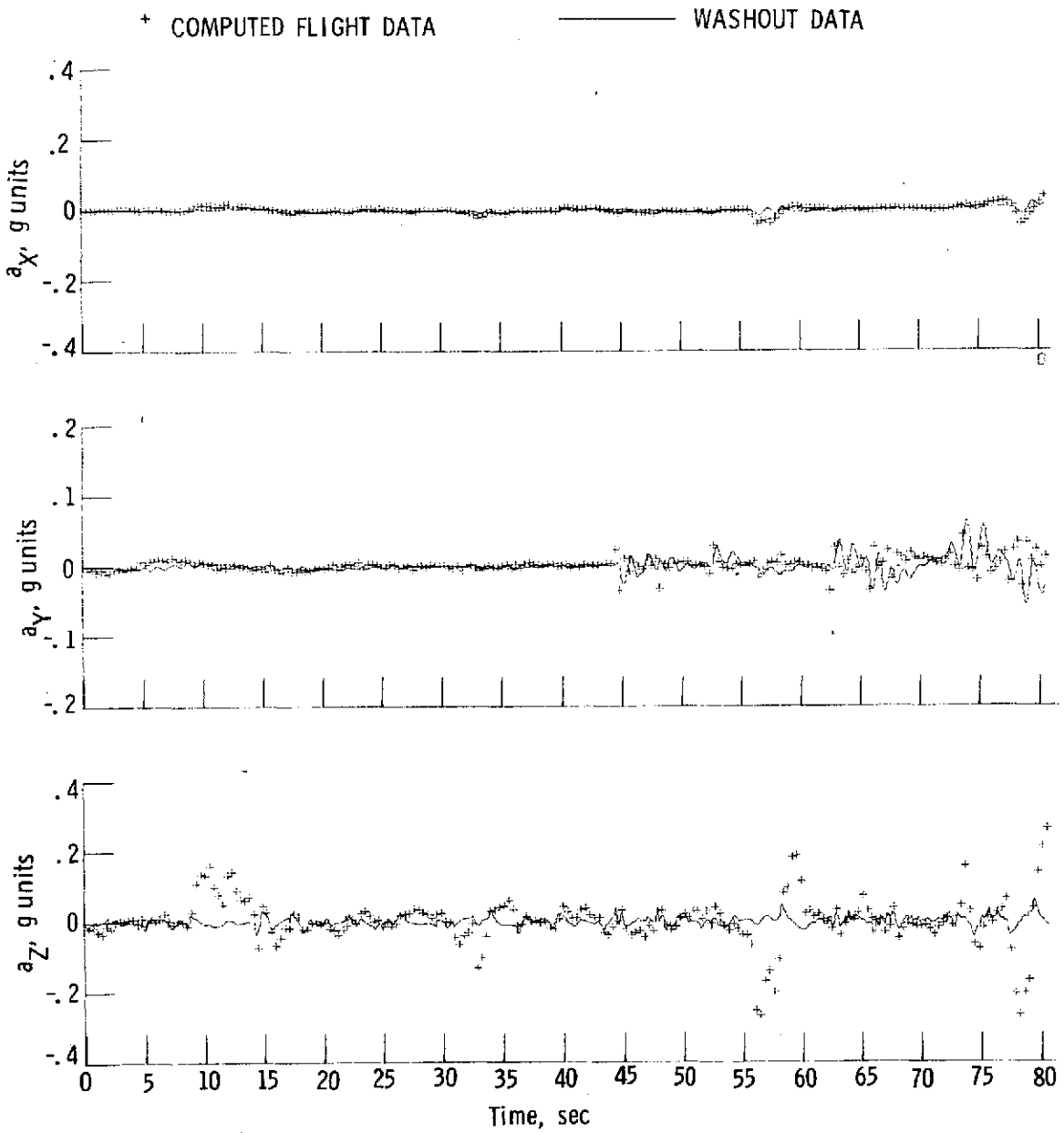
Figure 12.- Continued.
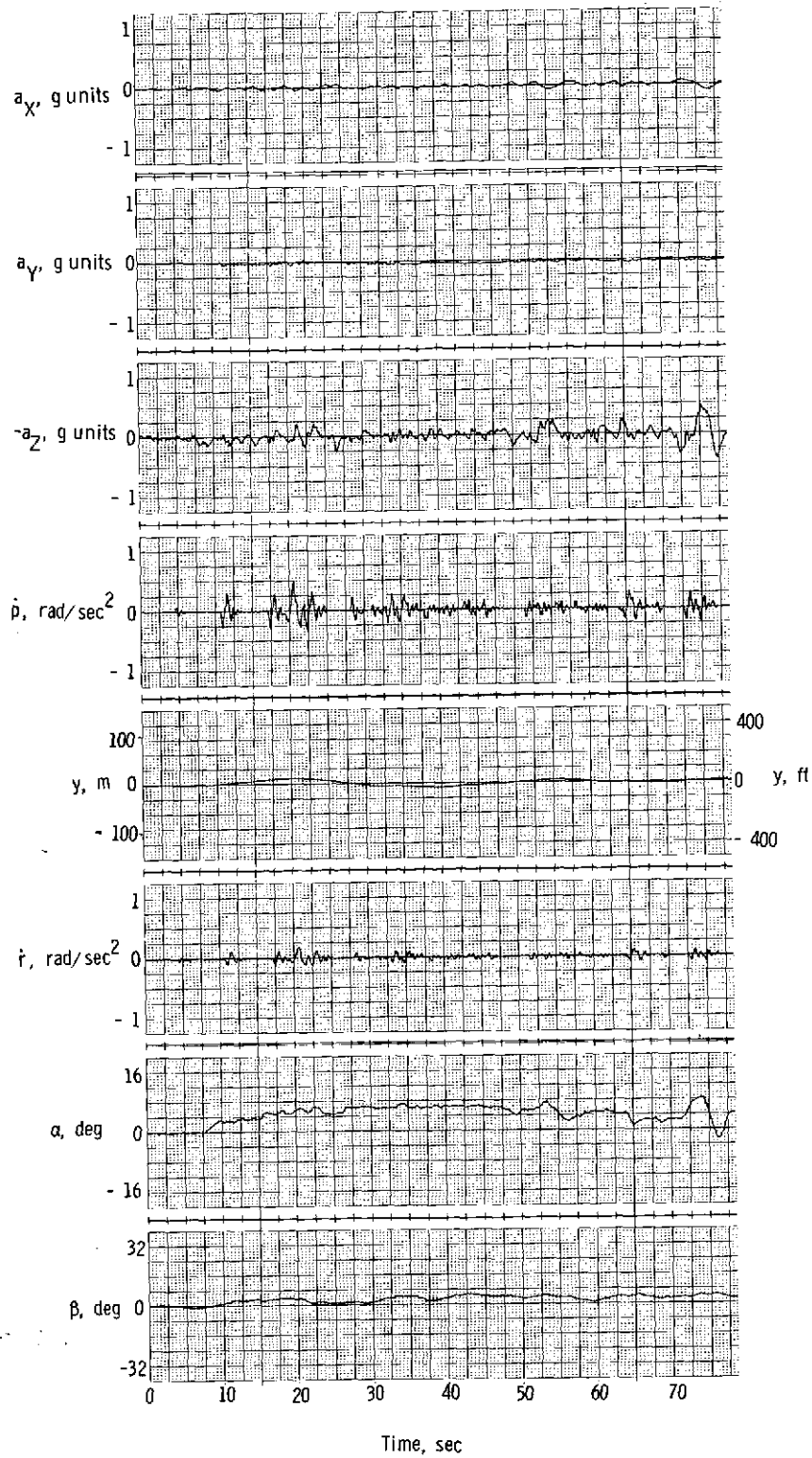
Figure 12.- Concluded.
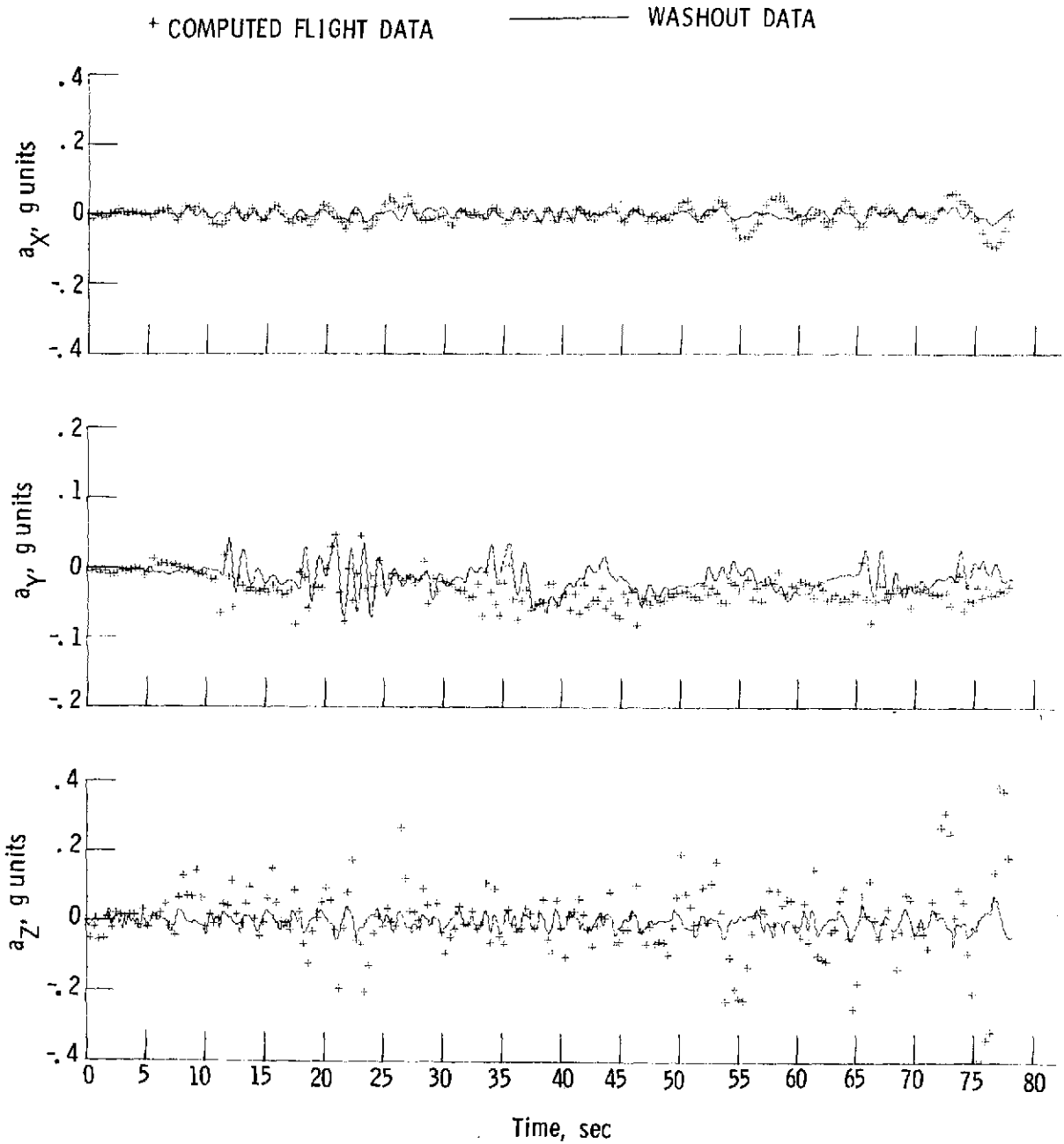
Figure 13.- Computed motion-base response to typical constant-speed two-segment approach in low-level turbulence.
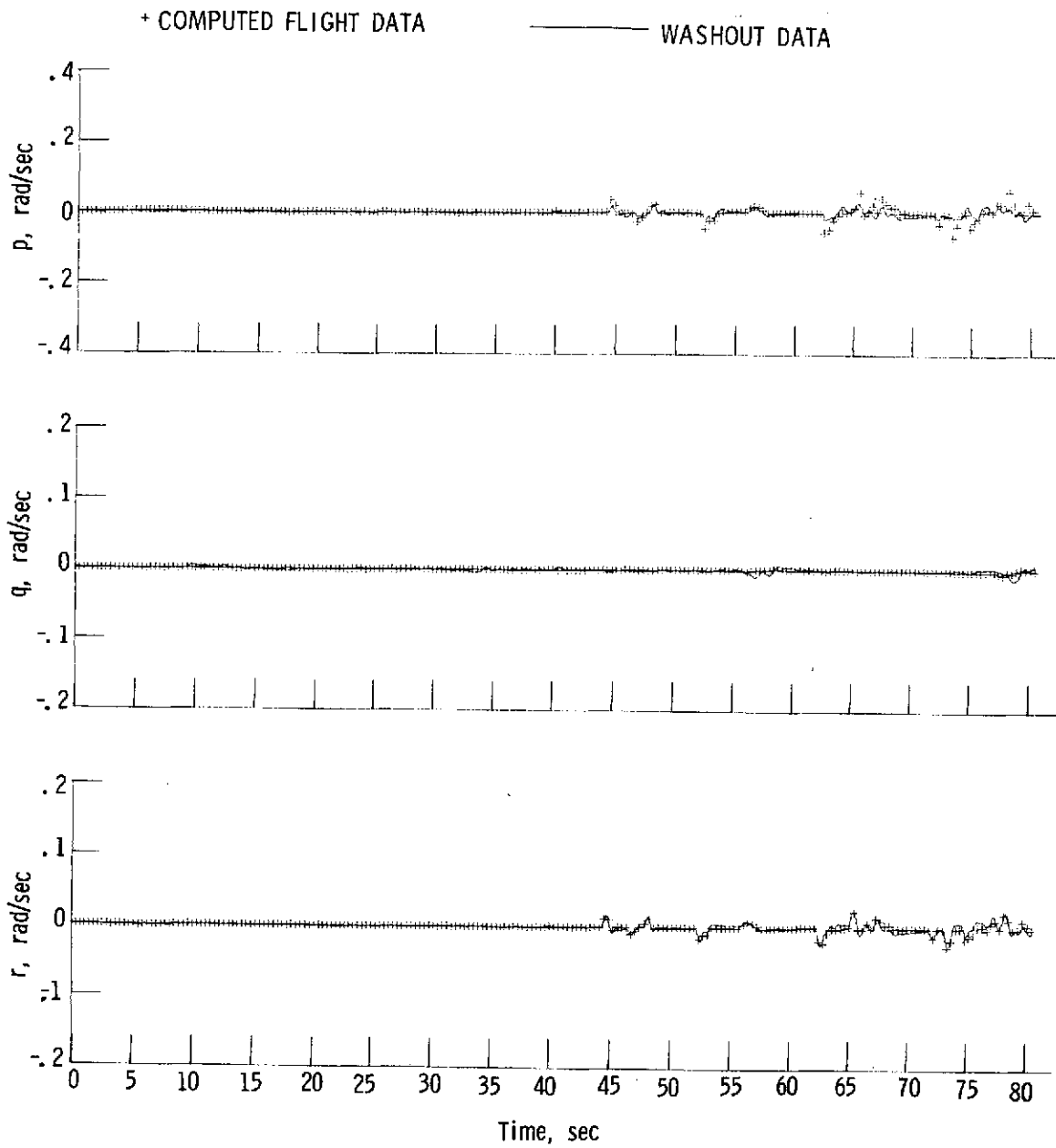
Figure 13.- Continued.

Figure 13.- Continued.
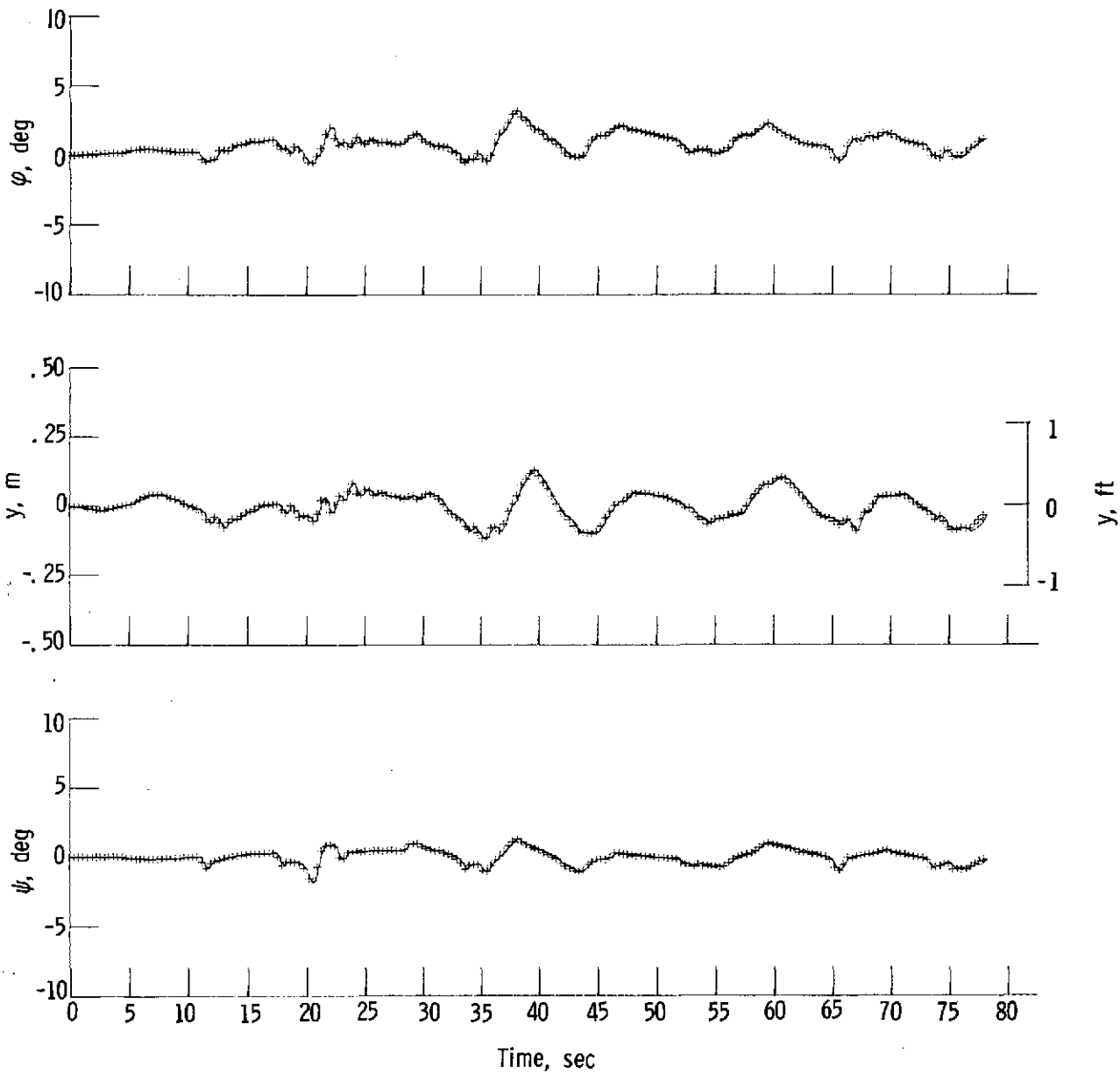
Figure 13.- Concluded.
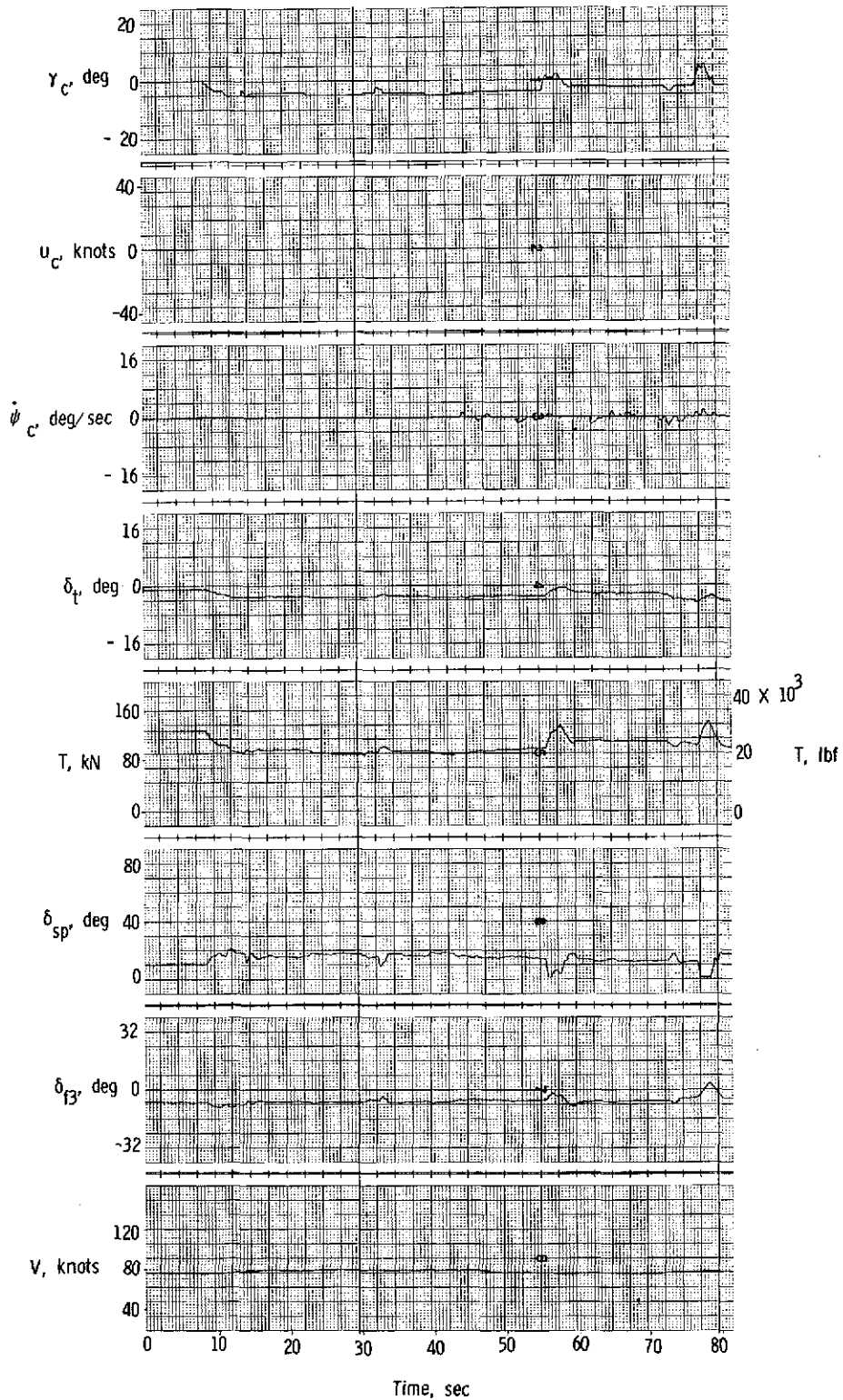
Figure 14.- Typical constant-speed two-segment approach with modified decoupled controls in low-level turbulence.
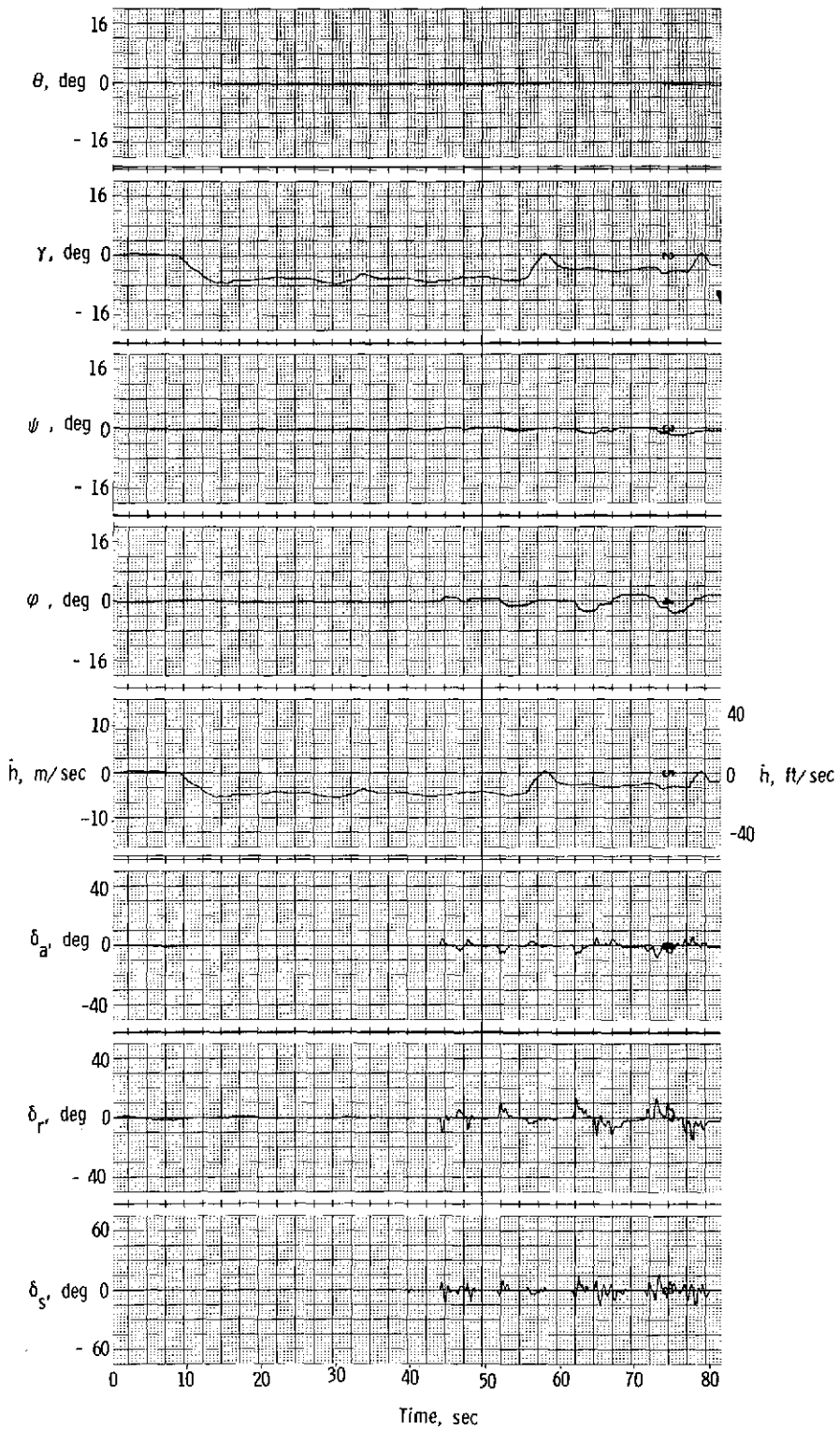
Figure 14.- Continued.
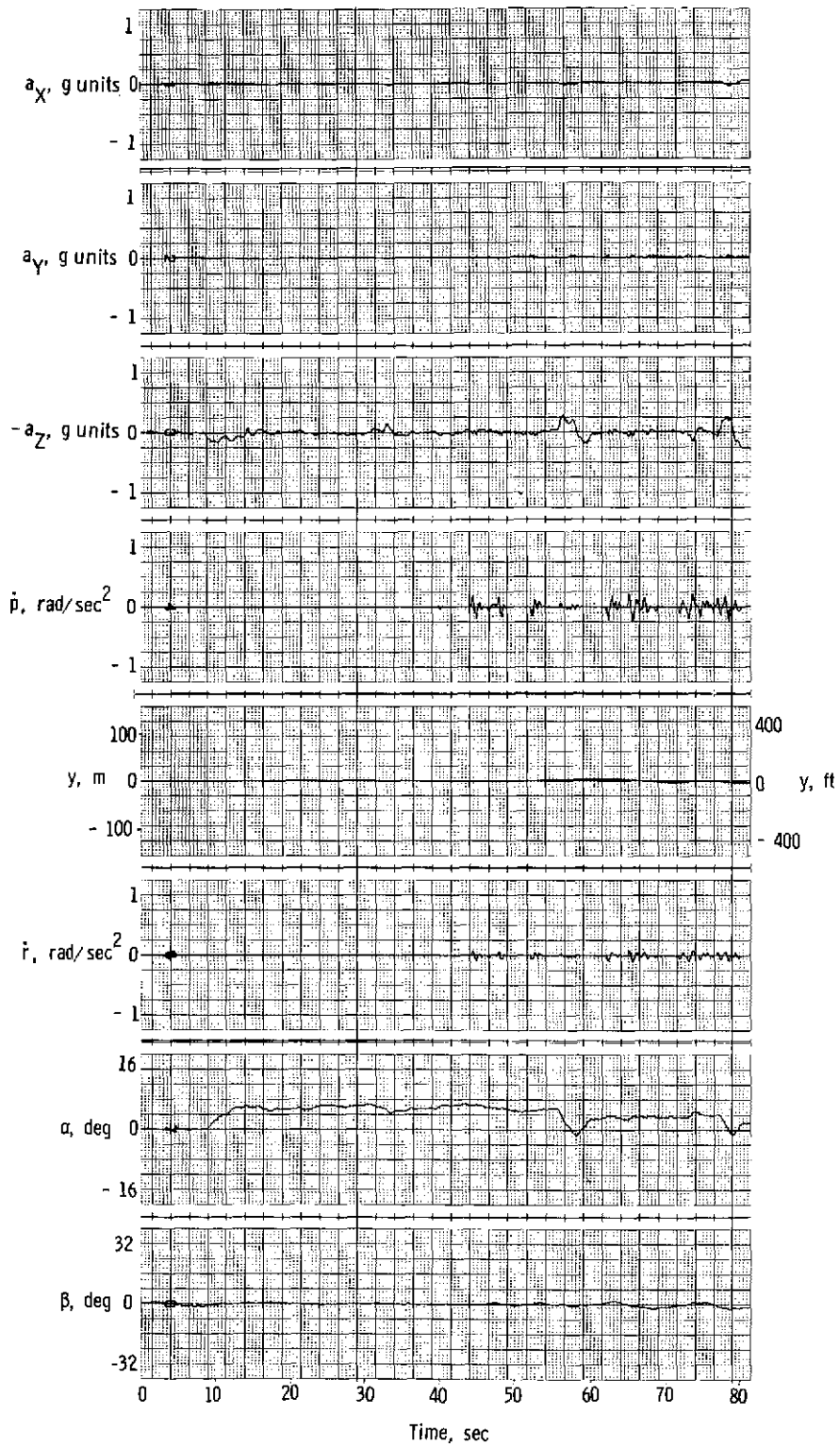
Figure 14.- Concluded.

Figure 15.- Computed motion-base response for typical constant-speed two-segment approach with modified decoupled controls in low-level turbulence.
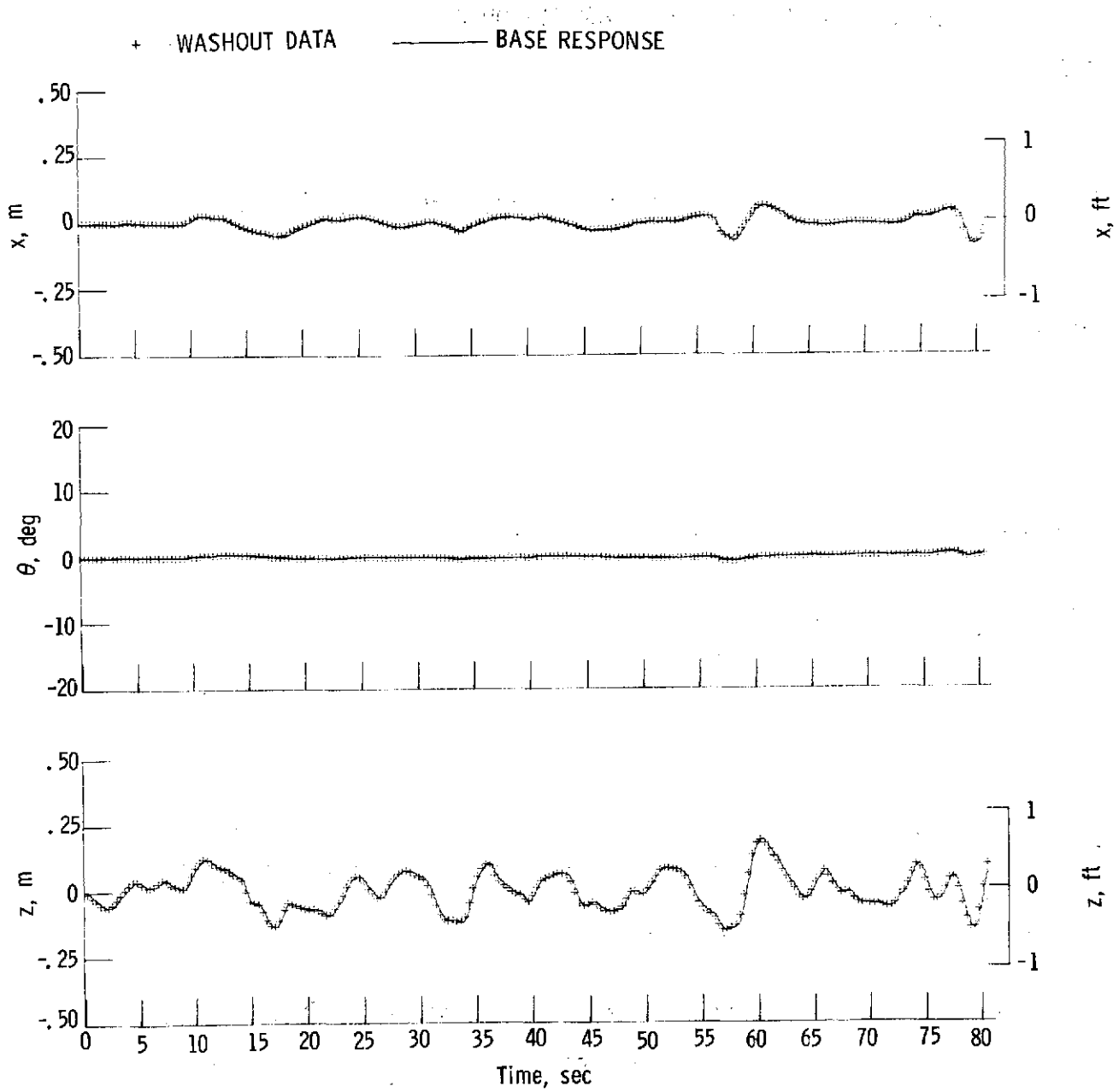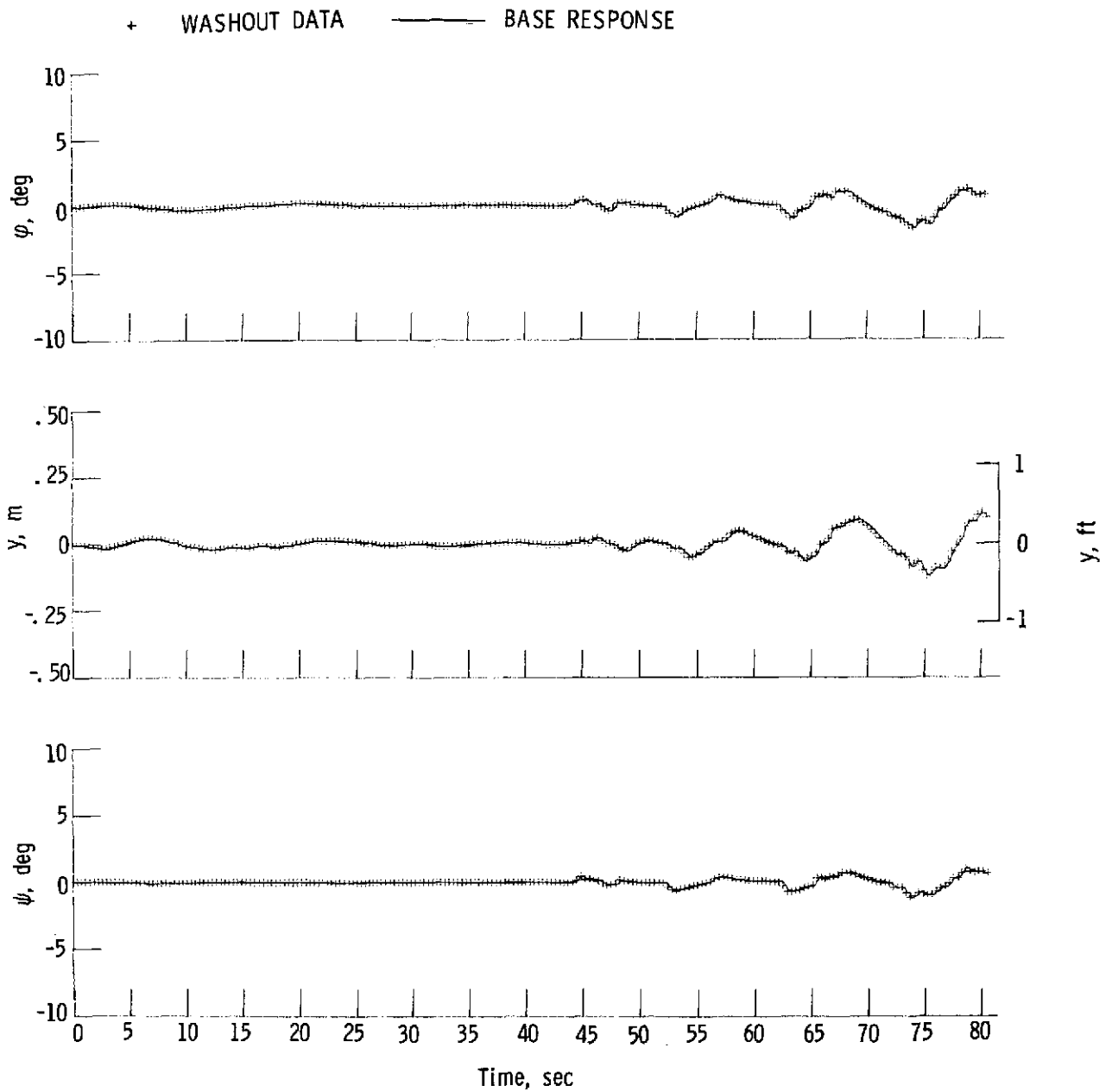
Figure 15.- Continued.

Figure 15.- Continued.

Figure 15.- Concluded.